$S_{11}-N(1535)$ and $-N(1650)$ resonances in meson-baryon unitarized coupled channel chiral perturbation theory

J. Nieves* and E. Ruiz Arriola†
Departamento de Fisica Moderna, Universidad de Granada, E-18071 Granada, Spain
(Received 27 April 2001; published 12 November 2001)

The *s*-wave meson-baryon scattering is analyzed for the strangeness $S=0$ sector in a Bethe-Salpeter coupled channel formalism incorporating chiral symmetry. Four channels have been considered: πN, ηN, $K\Lambda$, $K\Sigma$. The needed two-particle irreducible matrix amplitude is taken from lowest order chiral perturbation theory in a relativistic formalism and low energy constants are fitted to the elastic πN phase shifts and the $\pi^- p\to\eta n$ and $\pi^- p\to K^0\Lambda$ cross section data. The position of the complex poles in the second Riemann sheet of the scattering amplitude determines masses and widths of the $S_{11}-N(1535)$ and $-N(1650)$ resonances, in reasonable agreement with experiment. A good overall description of data, from πN threshold up to 2 GeV, is achieved, keeping in mind that the two-pion production channel has not been included.

DOI: 10.1103/PhysRevD.64.116008 PACS number(s): 11.10.St, 11.30.Rd, 11.80.Et

I. INTRODUCTION

The $N(1535)$ and $N(1650)$ resonances appear as outstanding features not only in elastic πN scattering in the strangeness zero S_{11} ($L_{2T,2J}$) partial wave but also in other meson-baryon reactions at intermediate energies. In quark model approaches these excited nucleon resonances are mainly composites of three valence quarks, and their widths are computed as matrix elements of hadronic transition operators. However, the description of hadron scattering reactions becomes cumbersome in this framework, and it requires quite elaborate techniques as the resonating group approach, where it becomes extremely difficult to impose chiral symmetry (CS) [1].

Renouncing to find out a picture of the hadron as a valence quark bound state, a different point of view consists of describing scattering reactions taking the hadrons as the relevant degrees of freedom at low energies. Then, resonances manifest themselves as poles of the scattering amplitude in a certain Riemann sheet in the complex energy plane. To perform such a program requires implementing unitarity in the model. A multichannel *K*-matrix method is used in the work of Ref. [2]. Though CS is not incorporated, this phenomenological approach is able to reproduce a large amount of data related to the $\pi N\to\pi N$ reaction. The three-body final state, two-pion production channel $\pi\pi N$ is incorporated through an effective use of two-body channels with higher mesonic and baryonic resonances. In this paper, we will work in this latter type of approaches, but explicitly imposing CS constraints as an indirect way of incorporating the bulk of the underlying quantum chromodynamics (QCD). Thus, we will establish a unitarity scheme based on the chiral perturbation theory (ChPT) amplitudes.

CS provides important constraints to the description of low energy hadronic processes and, in particular, to baryon-meson dynamics. There have been previous studies of the $\pi N-S_{11}$ partial wave using a coupled channel formalism and imposing CS constraints. In Ref. [3] a Schrödinger coupled channel treatment was employed and the additional inclusion of phenomenological hadronic form factors was invoked. Within this framework, the *p*-wave contribution has also been recently examined [4]. The two pion production channel is not considered in these works. Perturbative estimates [5–7] for the reaction $\pi N\to\pi\pi N$ indicate that this three-body channel keeps moderately small not only at threshold but also in a certain region above it. An attempt to include the two-pion production reaction can be found in Ref. [8], but the treatment of the $\pi\pi N$ channel is effective and it is represented by an unphysical two-body channel which represents all remaining processes.

In Ref. [9] the Bethe-Salpeter equation (BSE) has been employed in the spirit of an effective field theory (EFT). There, the $\pi\pi N$ channel is not considered either and the authors require the introduction of less renormalization constants than allowed by CS. Despite these restrictions, the model describes not only the elastic πN channel, but also the two-body inelastic ones in an energy window around the $N(1535)$ resonance. Nevertheless, it fails at threshold [10]. Given this partial success and the great technical difficulties to solve the BSE incorporating the three-body $\pi\pi N$ channel, one might wonder what features of the data can be explained incorporating CS constraints and restoring two-body unitarity.

In the present work we restrict our study to the nonstrange meson-baryon S_{11} partial wave and adopt a similar framework as in those references, but with some important differences. First, we will implement exact unitarity by solving the BSE taking the needed input from lowest order relativistic ChPT. A similar program has been successfully undertaken both in the pion-pion sector [11] and in the $\pi N-P_{33}$ partial wave [12]. Thus, we avoid the use of phenomenological form factors and all required information (low energy constants) can be, in principle, obtained from higher orders in the chiral expansion. Besides, we aim at describing not only

*Email address: jmnieves@ugr.es
†Email address: earriola@ugr.es

a narrow energy window, placed at threshold or in the neighborhood of some resonance, but also a wider energy region ranging from πN threshold up to almost a center of mass (c.m.) meson-baryon energy of $\sqrt{s}=2$ GeV.

As we discussed at length in Ref. [11] the BSE, in the context of EFT's, can be solved in two different schemes: off shell and on shell. Here, we use the off-shell scheme because of the lack of information on the next-to-leading order in the chiral expansion. In this scheme, the on-shell scattering amplitude requires some knowledge of the off-shell behavior of the two-particle irreducible amplitude (*potential*). After renormalization of the amplitude this off-shell input leads to a finite number of phenomenological constants which encode the detailed underlying short-distance dynamics. In practice, these constants can be either fitted to experiment or determined by matching the resulting Bethe-Salpeter (BS) amplitude to standard ChPT.[1] Obviously, the method of determining the constants by matching to ChPT seems a better one than a direct fit to experimental data.[2] For the case of meson-baryon scattering, the only known information coming from ChPT involves tree-level amplitudes and free propagators; there is no possibility to compare with ChPT beyond leading order and thus one is forced to fit the unknown low energy constants (LEC's) to data.

As is the case in the purely mesonic sector, the off-shell scheme generates a rich structure of unknown constants which allow for a good description of the amplitudes. Although the appearance of more undetermined constants may appear a less predictive approach as, say, putting a cutoff (one single parameter) in the divergent integrals as is done in Ref. [9], it reflects the real state of the art of our lack of knowledge on underlying QCD dynamics. The number of adjustable LEC's should not be smaller than those allowed by symmetry; this is the only way both to falsify all possible theories embodying the same symmetry principles and to make wider the energy window which is being described. Limiting such a rich structure allowed by CS results in a poor description of experimental data.

Before going further we would like also to say a word on the opposite situation, i.e., the possibility of having more low energy parameters than one actually needs. A possible redundancy of parameters is obviously an undesirable situation. In standard ChPT the number of LEC's is controlled to any order of the calculation by crossing and unitarity. Moreover, the dependence of the observables on them is strictly linear, so that it becomes possible to detect such a redundant combination in case it occurs.[3] In a unitarized approach, the only way to avoid this parameter redundancy is to match the unitarized amplitude to the standard ChPT amplitude. As we have already said, there is no standard one-loop ChPT calculation for the S_{11} partial wave of the meson-baryon reaction with open channels to compare with. An indirect way to detect such a parameter redundancy might be through a fit to experimental data if the errors in some parameters turn out to be very large.

We have considered four coupled channels: πN, ηN, $K\Lambda$, $K\Sigma$ and taken into account $SU(3)$-breaking symmetry effects but neglected the considerably smaller isospin violation ones. We have found that CS allows for a solution of the BSE which is flexible enough to describe the elastic πN phase shifts, and the $\pi^- p\to\eta n$ and $\pi^- p\to K^0\Lambda$ cross section data from threshold to c.m. energies well above the $N(1650)$ resonance. Besides the rest of elastic and inelastic two-body reaction channels[4] implicit in the adopted formalism come as predictions of the model. The position of the complex poles in the second Riemann sheet of the amplitudes determines masses and widths of the $S_{11}-N(1535)$ and $-N(1650)$ resonances, which turn out to be in reasonable agreement with experiment. Preliminary results were presented in [18].

The paper is organized as follows: In Sec. II we present the basic formalism used along the paper. We start with the chiral Lagrangian relevant to our calculation, from which the lowest order meson-baryon two-particle irreducible matrix amplitude is deduced. After presenting our notations for the coupled channel kinematics we discuss the basic pertinent features of the BSE for *s*-wave meson-baryon scattering. Using the amplitude from lowest order ChPT as the potential, we solve and renormalize the BSE in the spirit of an EFT. In Sec. III we present our numerical results, together with a detailed discussion on the fitting procedure and Monte Carlo propagation of inherited error bars to all possible reaction channels. The quantum field theoretical interpretation of resonances as unstable particles requires determining their mass and width as poles in a unphysical Riemann sheet. In our case there are 16 sheets which we discuss in some detail, and we search for the most important pole singularities. Error estimates are made in terms of the available experimental uncertainties in the phase shifts and amplitudes. Finally, in Sec. IV we present some conclusions and outlook for future work.

[1]Ideally, these phenomenological parameters should be computed from first principles, a yet impossible task.

[2]In addition, if the matching is possible the off-shell scheme becomes unnecessarily complicated, as compared to other methods directly unitarizing the final on-shell amplitude given in terms of the standard low energy constants. For details, on the on-shell BSE approach or on the inverse amplitude method (IAM) for meson-meson scattering see, for instance, the thorough discussion in the second entry of Ref. [11]. For πN elastic scattering, recent IAM studies have been pursued in Refs. [13] and [14].

[3]A good example of this is $\pi\pi$ scattering to two loops ([15,16]) where one gets, besides the four one-loop parameters $\bar{l}_{1,2,3,4}$, six new parameters but in redundant combinations. Instead, it is customary to use the six $\bar{b}_{1,2,3,4,5,6}$ independent combinations, which depend on the one-loop $\bar{l}$'s and the six new two loop parameters and contain mixed orders. Such a situation also takes place in πN scattering in heavy baryon ChPT (HBChPT) at fourth order [17].

[4]Each of the entries of the 4×4 matrix solution of the BSE is the *T*-scattering amplitude for a meson-baryon reaction constructed out of the four considered channels: $\pi N\to\pi N$, $\pi N\to\eta N$, $\pi N\to K\Lambda$, $\pi N\to K\Sigma$, $\eta N\to\eta N$, $\eta N\to K\Lambda$, $\eta N\to K\Sigma$, $K\Lambda\to K\Lambda$, $K\Lambda\to K\Sigma$, $K\Sigma\to K\Sigma$ and the reverse processes.

II. THEORETICAL FRAMEWORK

A. Chiral baryon-meson Lagrangian

At lowest order in the chiral expansion the chiral baryon-meson Lagrangian contains kinetic and mass baryon pieces and meson-baryon interaction terms and is given by [19]

$$\mathcal{L}_1 = \mathrm{Tr}\{\bar{B}(\mathrm{i}\nabla\!\!\!\!/ - M_B)B\} + \tfrac{1}{2}\mathcal{D}\,\mathrm{Tr}\{\bar{B}\gamma^\mu\gamma_5\{u_\mu, B\}\} + \tfrac{1}{2}\mathcal{F}\,\mathrm{Tr}\{\bar{B}\gamma^\mu\gamma_5[u_\mu, B]\}. \quad (1)$$

The meson kinetic and mass pieces and the baryon mass chiral corrections are second order and read

$$\mathcal{L}_2 = \frac{f^2}{4}\mathrm{Tr}\{u_\mu^\dagger u^\mu + (U^\dagger\chi + \chi^\dagger U)\} - b_0\,\mathrm{Tr}(\chi_+)\mathrm{Tr}(\bar{B}B) - b_1\,\mathrm{Tr}(\bar{B}\chi_+ B) - b_2\,\mathrm{Tr}(\bar{B}B\chi_+) \quad (2)$$

where "Tr" stands for the trace in $SU(3)$. In addition,

$$\nabla_\mu B = \partial_\mu B + \tfrac{1}{2}[u^\dagger\partial_\mu u + u\partial_\mu u^\dagger, B],$$

$$U = u^2 = e^{\mathrm{i}\sqrt{2}\Phi/f}, \quad u_\mu = \mathrm{i}u^\dagger\partial_\mu U u^\dagger,$$

$$\chi_+ = u^\dagger\chi u^\dagger + u\chi^\dagger u, \quad \chi = 2B_0\mathcal{M}. \quad (3)$$

M_B is the common mass of the baryon octet, due to spontaneous chiral symmetry breaking for massless quarks. The $SU(3)$ coupling constants which are determined by semileptonic decays of hyperons are $\mathcal{F}\sim 0.46$, $\mathcal{D}\sim 0.79$ ($\mathcal{F}+\mathcal{D}=g_A=1.25$). The constants B_0 and f (pion weak decay constant in the chiral limit) are not determined by the symmetry. The current quark mass matrix is $\mathcal{M}=\mathrm{Diag}(m_u, m_d, m_s)$. The parameters b_0, b_1, and b_2 are coupling constants with dimension of an inverse mass. The values of b_1 and b_2 can be determined from baryon mass splittings, whereas b_0 gives an overall contribution to the octet baryon mass M_B. The $SU(3)$ matrices for the meson and the baryon octet are written in terms of the meson and baryon spinor fields, respectively, and are given by[5]

$$\Phi = \begin{pmatrix} \frac{1}{\sqrt{2}}\pi^0 + \frac{1}{\sqrt{6}}\eta & \pi^+ & K^+ \\ \pi^- & -\frac{1}{\sqrt{2}}\pi^0 + \frac{1}{\sqrt{6}}\eta & K^0 \\ K^- & \bar{K}^0 & -\frac{2}{\sqrt{6}}\eta \end{pmatrix}, \quad (4)$$

and

$$B = \begin{pmatrix} \frac{1}{\sqrt{2}}\Sigma^0 + \frac{1}{\sqrt{6}}\Lambda & \Sigma^+ & p \\ \Sigma^- & -\frac{1}{\sqrt{2}}\Sigma^0 + \frac{1}{\sqrt{6}}\Lambda & n \\ \Xi^- & \Xi^0 & -\frac{2}{\sqrt{6}}\Lambda \end{pmatrix}, \quad (5)$$

respectively. The $MB\to MB$ vertex obtained from the former Lagrangian reads[6]

$$\mathcal{L}_{MB\to MB} = \frac{\mathrm{i}}{4f^2}\mathrm{Tr}\{\bar{B}\gamma^\mu[[\Phi, \partial_\mu\Phi], B]\}. \quad (6)$$

Assuming isospin conservation, the scattering amplitude[7] in the Dirac spinor basis, whose relation to the cross section is given in Sec. II B, at lowest order is given by

$$t_P^{(1)}(k,k') = \frac{D}{f^2}(k\!\!\!/ + k\!\!\!/'), \quad (7)$$

where k and k' are incoming and outgoing meson momenta and D a coupled-channel matrix. For strangeness $S=0$ and isospin $T=1/2$ the coupled channel matrix D reads[8]

$$D_{S=0}^{T=1/2} = \frac{1}{4}\begin{array}{c} \begin{matrix} \pi N & \eta N & K\Lambda & K\Sigma \end{matrix} \\ \begin{pmatrix} -2 & 0 & -3/2 & +1/2 \\ 0 & 0 & +3/2 & +3/2 \\ -3/2 & +3/2 & 0 & 0 \\ +1/2 & +3/2 & 0 & -2 \end{pmatrix} \end{array} \begin{matrix} \pi N \\ \eta N \\ K\Lambda \\ K\Sigma \end{matrix}. \quad (8)$$

While amplitudes follow the chiral symmetry breaking pattern from the effective Lagrangian to a good approximation, it is well known that physical mass splittings have an important influence when calculating the reaction phase space. Indeed, the correct location of reaction thresholds requires taking physical masses for the corresponding reaction channels. We have taken into account this effect in our numerical calculation. Besides, chiral corrections to the amplitudes also incorporate explicit CS breaking effects in addition to those already present in the Lagrangians above. In practice, we use different numerical values for f_π, f_K, and

[5]For the purpose of our work we do not consider any mixing between octet and singlet $SU(3)$ representations.

[6]We have omitted the pieces proportional to the couplings $\mathcal{D}$ and $\mathcal{F}$ because they do not contribute to s wave. On the other hand, the Lagrangian below does not lead to a pure s-wave contribution and a further projection will be required.

[7]We use the convention, in symbolic notation, $-iT_{MB\to MB} = +i\mathcal{L}_{MB\to MB}$.

[8]There is a mistake in the relative phases of Ref. [3]. We thank A. Ramos for confirming this point to us. We use the isospin phase convention of Ref. [20]: negative phases for the isospin states $-|\pi^+\rangle$, $-|\bar{K}_0\rangle$, $-|\Sigma^+\rangle$, $-|\bar{\Xi}^-\rangle$, $-|\bar{\Sigma}^-\rangle$, $-|\bar{n}\rangle$.

f_η, as it is discussed in Sec. III. This can be easily accomplished through the prescription

$$D/f^2 \to \hat{f}^{-1} D \hat{f}^{-1}, \quad \hat{f} \equiv \mathrm{Diag}(f_\pi, f_\eta, f_K, f_K). \tag{9}$$

For simplicity and a more clear bookkeeping of chiral order dependences we will use the D/f^2 notation throughout the paper, meaning Eq. (9) in practice.

B. Scattering amplitude and kinematics

The coupled channel scattering amplitude for the baryon-meson process in the isospin channel, $T=\frac{1}{2}$,

$$B(M_A, P-k, s_A) + M(m_A, k) \to B(M_B, P-k', s_B) + M(m_B, k') \tag{10}$$

with baryon (meson) masses M_A and M_B(m_A and m_B) and spin indices (helicity, covariant spin, etc. . . . .) s_A, s_B, is given by

$$T_P[B\{k', s_B\} \leftarrow A\{k, s_A\}] = \overline{u}_B(P-k', s_B) t_P(k,k') \times u_A(P-k, s_A). \tag{11}$$

Here, $u_A(P-k, s_A)$ and $u_B(P-k', s_B)$ are baryon Dirac spinors[9] for the ingoing and outgoing baryons, respectively, P is the conserved total four-momentum and $t_P(k,k')$ is a matrix in the Dirac and coupled channel spaces. On the mass shell and using the equations of motion for the free Dirac spinors $(\not{P}-\not{k}-M_A)u_A(P-k)=0$ and its transposed $\overline{u}_A(P-k)(\not{P}-\not{k}-M_A)=0$ the parity and Lorentz invariant amplitude t_P can be written as

$$t_P(k,k')|_{\text{on shell}} = t_1(s,t)\not{P} + t_2(s,t) \tag{12}$$

with $s=P^2=\not{P}^2$, $t=(k-k')^2$, and t_1 and t_2 matrices in the coupled channel space. The normalization of the amplitude T_P is determined by its relation to the c.m. differential cross section, and it is given above threshold, $s > \max\{(M_A+m_A)^2, (M_B+m_B)^2\}$, by

$$\frac{d\sigma}{d\Omega}[B\{k_B, s_B\} \leftarrow A\{k_A, s_A\}] = \frac{1}{64\pi^2 s} \frac{|\vec{k}_B|}{|\vec{k}_A|} |T_P[B\{k_B, s_B\} \leftarrow A\{k_A, s_A\}]|^2. \tag{13}$$

Rotational, parity, and time-reversal invariances ensure for the on-shell particles

$$T_P[\{k_B, s_B\} \leftarrow \{k_A, s_A\}] = -8\pi\sqrt{s} \sqrt{\frac{|\vec{k}_A|}{|\vec{k}_B|}} \{\mathcal{A}(s,\theta)\delta_{s_A s_B} + i\mathcal{B}(s,\theta)(\hat{n}\cdot\vec{\sigma})_{s_B s_A}\}. \tag{14}$$

$\mathcal{A}$ and $\mathcal{B}$ are matrices in the coupled channel space, θ the c.m. angle between the initial and final meson three-momenta and $\hat{n}$ a unit three-vector orthogonal to $\vec{k}_A$ and $\vec{k}_B$. Partial waves (matrices in the coupled channel space), $f_L^J(s)$, are related to $\mathcal{A}, \mathcal{B}$ by [21]

$$\mathcal{A}(s,\theta) = \sum_L [(L+1) f_L^{L+1/2}(s) + L f_L^{L-1/2}(s)] P_L(\cos\theta),$$

$$\mathcal{B}(s,\theta) = -\sum_L [f_L^{L+1/2}(s) - f_L^{L-1/2}(s)] \frac{dP_L(\cos\theta)}{d\theta}. \tag{15}$$

In terms of the matrices t_1 and t_2 defined in Eq. (12), the s-wave coupled-channel matrix, $f_0^{1/2}(s)$, is given by

$$[f_0^{1/2}(s)]_{B\leftarrow A} = -\frac{1}{8\pi\sqrt{s}} \sqrt{\frac{|\vec{k}_B|}{|\vec{k}_A|}} \sqrt{E_B+M_B}\sqrt{E_A+M_A} \times \left[\frac{1}{2}\int_{-1}^{1} d\cos\theta [\sqrt{s} t_1(s,t) + t_2(s,t)]_{BA}\right], \tag{16}$$

where the c.m. three-momentum moduli read

$$|\vec{k}_i| = \frac{\lambda^{1/2}(s, M_i, m_i)}{2\sqrt{s}}, \quad i = A, B \tag{17}$$

with $\lambda(x,y,z) = x^2+y^2+z^2-2xy-2xz-2yz$ and $E_{A,B}$ the baryon c.m. energies. The phase of the matrix T_P is such that the relation between the diagonal elements $(A=B)$ in the coupled channel space of $f_0^{1/2}(s)$ and the inelasticities (η) and phase shifts (δ) is the usual one,

$$[f_0^{1/2}(s)]_{AA} = \frac{1}{2i|\vec{k}_A|}[\eta_A(s) e^{2i\delta_A(s)} - 1]. \tag{18}$$

Hence, the optical theorem reads, for $s \geqslant (M_A+m_A)^2$,

$$\frac{4\pi}{|\vec{k}_A|} \mathrm{Im}[f_0^{1/2}(s)]_{AA} = \sum_B \sigma_{B\leftarrow A} = 4\pi \sum_B |[f_0^{1/2}(s)]_{BA}|^2 = \sigma_{AA} + \frac{\pi}{|\vec{k}_A|^2}(1-\eta_A^2), \tag{19}$$

where in the right-hand side only open channels contribute.

C. Bethe-Salpeter equation

The Bethe-Salpeter equation reads

$$t_P(k,k') = v_P(k,k') + i\int \frac{d^4q}{(2\pi)^4} t_P(q,k')\Delta(q) \times S(P-q) v_P(k,q), \tag{20}$$

where $t_P(k,k')$ is the scattering amplitude defined in Eq. (11), $v_P(k,k')$ is the two-particle irreducible Green's function (or *potential*), and $S(P-q)$ and $\Delta(q)$ are the baryon

[9] We use the normalization $\overline{u}u = 2M$.

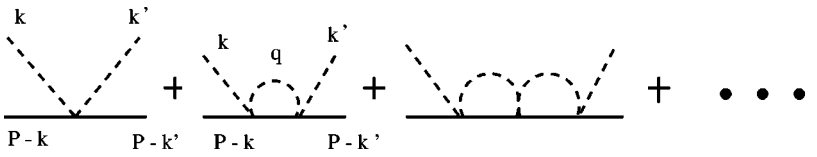

FIG. 1. Diagrams summed by the Bethe-Salpeter equation at lowest order. Kinematics defined in the main text.

and meson exact propagators, respectively. The above equation turns out to be a matrix one, both in the coupled channel and Dirac spaces. The resulting scattering amplitude $t_P(k,k')$ fulfills the coupled channel unitarity condition

$$t_P(k,k')-\overline{t}_P(k',k)=-\mathrm{i}(2\pi)^2\int\frac{d^4q}{(2\pi)^4}t_P(q,k')\times\delta^+[q^2-\hat{m}^2](\not P-\not q+\hat{M})\times\delta^+[(P-q)^2-\hat{M}^2]\overline{t}_P(q,k) \tag{21}$$

where $\overline{t}_P(k,p)=\gamma_0 t_P^\dagger(k,p)\gamma_0$ and $t_P^\dagger(k,p)$ stands for the total adjoint in the Dirac and coupled channel spaces (including also the change $s+\mathrm{i}\epsilon\to s-\mathrm{i}\epsilon$) and $\hat{m}$ and $\hat{M}$ the meson and baryon (diagonal) mass matrices, respectively. Finally, $\delta^+(p^2-m^2)=\Theta(p^0)\delta(p^2-m^2)$, Θ being the Heaviside step function.

If the on-shell amplitude depends only on the total momentum[10] P, $t_P(k,k')|_{\text{on shell}}=t(\not P)$, as will be the case below, the unitarity condition can be rewritten in a much simpler and useful form as a discontinuity equation above the corresponding physical thresholds

$$\mathrm{Disc}[t(\not P)^{-1}]=-\mathrm{Disc}[J(\not P)]\quad\text{with}$$

$$\mathrm{Disc}[A(s)]\equiv A(s+\mathrm{i}\epsilon)-A(s-\mathrm{i}\epsilon) \tag{22}$$

where the quadratic and logarithmically divergent integral

$$J(\not P)=\mathrm{i}\int\frac{d^4q}{(2\pi)^4}\frac{1}{q^2-\hat{m}^2}\frac{1}{\not P-\not q-\hat{M}} \tag{23}$$

has been introduced and Cutkosky's rules used to evaluate its discontinuity. This integral is treated in detail in Appendix A. As usual, we take the $\mathrm{i}\epsilon$ prescription $\hat{m}^2\to\hat{m}^2-\mathrm{i}\epsilon$ and $\hat{M}\to\hat{M}-\mathrm{i}\epsilon$ which we implicitly assume in the sequel.

D. Solution of the BSE equation at lowest order

The BSE requires some input potential and baryon and meson propagators to be solved. We proceed here along the lines proposed in previous work [11] and use a chiral expansion to determine both the potential and propagator. From the chiral Lagrangian one gets at lowest order [Eq. (7)]

$$v_P(k,k')=t_P^{(1)}(k,k')=\frac{D}{f^2}(\not k+\not k') \tag{24}$$

with D the coupled-channel matrix, which was given in Eq. (8). The propagators at lowest order are simply the free ones,

$$\Delta(q)=\frac{1}{q^2-\hat{m}^2},\quad S(P-q)=\frac{1}{\not P-\not q-\hat{M}} \tag{25}$$

which are diagonal in the coupled channel space. Once we have approximate expressions for both the *potential* and the meson and baryon propagators, we proceed to exactly solve the BSE. The second order Born approximation to the solution of the BSE [i.e., approximating $t_P(q,k')$ in the kernel of the equation by $v_P(q,k')$] suggests the following form for the exact solution:

$$t_P(k,k')=a(\not P)+\not k' b_R(\not P)+b_L(\not P)\not k+\not k' c(\not P)\not k, \tag{26}$$

where a, b_R, b_L, and c are Lorentz scalar matrices in the Dirac and the coupled channel spaces. At this lowest order of the BSE approach, these matrices only depend on $\not P$, thus they turn out to be independent of the Mandelstam variable t.

Such an amplitude contains an infinite sum of diagrams, as shown in Fig. 1, but does not contain *all* possible one-loop dependences, for instance those coming from vertex renormalization. On the mass shell we may set $\not k\to\not P-\hat{M}$ and $\not k'\to\not P-\hat{M}$. Hence, thanks to the equations of motion the on-shell amplitude becomes a function of the total momentum $\not P$ and reads

$$t(\not P)=a+(\not P-\hat{M})b_R+b_L(\not P-\hat{M})+(\not P-\hat{M})c(\not P-\hat{M}), \tag{27}$$

where the explicit dependence on $\not P$ of the a,b_R,b_L,c matrix functions has been suppressed for simplicity.

Plugging the ansatz for the off-shell amplitude, $t_P(k,k')$, as given in Eq. (26) into the BSE equation and after some algebraic manipulations described in detail in Appendix B, we get for the inverse on-shell amplitude

$$t(\not P)^{-1}=-J(\not P)+\frac{\Delta_{\hat{m}}}{\not P-\hat{M}}+A^{-1},$$

$$A=\frac{1}{f^2}\{\not P-\hat{M},D\}_+ +\frac{1}{f^4}(\not P-\hat{M})D\frac{\Delta_{\hat{m}}}{\not P-\hat{M}}D(\not P-\hat{M})=\mu(s)+\nu(s)\not P,$$

[10] That is to say, the functions t_1 and t_2 in Eq. (12) do not depend on the Mandelstam variable t.

$$\mu(s)=\frac{1}{f^4}\Bigg\{-[D,\hat{M}]\frac{\hat{M}\Delta_{\hat{m}}}{s-\hat{M}^2}[D,\hat{M}]-f^2\{\hat{M},D\}_+ - D\Delta_{\hat{m}}D\hat{M}+[D,\hat{M}]\Delta_{\hat{m}}D\Bigg\},$$

$$\nu(s)=\frac{1}{f^4}\Bigg\{-[\hat{M},D]\frac{\Delta_{\hat{m}}}{s-\hat{M}^2}[\hat{M},D]+D\Delta_{\hat{m}}D+2f^2D\Bigg\}. \tag{28}$$

As we can see, the on-shell unitarity condition expressed in Eq. (22) is manifestly fulfilled. To proceed further we can decompose the inverse on-shell amplitude in the form

$$t(\not{p})^{-1}=K_1(s)\not{p}+K_2(s), \tag{29}$$

where $K_1(s)$ and $K_2(s)$ are matrices in the coupled channel space. Straightforward calculation yields

$$K_1(s)=-\frac{s-\hat{m}^2+\hat{M}^2}{2s}J_0(s)+\frac{\Delta_{\hat{m}}}{s-\hat{M}^2}-\frac{\Delta_{\hat{m}\hat{M}}}{2s}+(\nu s-\mu\nu^{-1}\mu)^{-1},$$
$$K_2(s)=-\hat{M}J_0(s)+\frac{\hat{M}\Delta_{\hat{m}}}{s-\hat{M}^2}-(\nu s\mu^{-1}\nu-\mu)^{-1}. \tag{30}$$

Thus, the amplitude can be written in the form of Eq. (12):

$$t(\not{p})=t_1(s)\not{p}+t_2(s) \tag{31}$$

with

$$t_1=(K_1 s-K_2K_1^{-1}K_2)^{-1},$$
$$t_2=(K_2-K_1K_2^{-1}K_1 s)^{-1}. \tag{32}$$

As we already said, when the two-particle irreducible amplitude v_P and the meson and baryon propagators entering in the BSE, the lowest ChPT order ones are taken, the matrices (in the coupled channel spaces) t_1 and t_2 turn out to be independent of the t-Mandelstam variable.[11] Hence the angle integral in Eq. (16) becomes trivial and apart from kinematical factors, the relevant combination entering in the s-wave scattering amplitude is

$$t(s)=t_1(s)\sqrt{s}+t_2(s)=[K_1(s)\sqrt{s}+K_2(s)]^{-1}. \tag{33}$$

After some algebraic reshuffling the expression for the inverse coupled channel matrix amplitude can conveniently be written as

$$t(s)^{-1}=-\frac{(\sqrt{s}+\hat{M})^2-\hat{m}^2}{2\sqrt{s}}\hat{J}_0(s)+\frac{\Delta_{\hat{m}}}{\sqrt{s}-\hat{M}}-\frac{\Delta_{\hat{m}\hat{M}}}{2\sqrt{s}} +\left[\frac{1}{f^2}\{\sqrt{s}-\hat{M},D\}_+ +\frac{1}{f^4}(\sqrt{s}-\hat{M})D\frac{\Delta_{\hat{m}}}{\sqrt{s}-\hat{M}}\times D(\sqrt{s}-\hat{M})\right]^{-1}. \tag{34}$$

Finally, the s-wave coupled-channel matrix amplitude $f_0^{1/2}(s)$ reads

$$[f_0^{1/2}(s)]_{BA}=-\frac{1}{8\pi\sqrt{s}}\sqrt{\frac{|\vec{k}_B|}{|\vec{k}_A|}}\sqrt{E_B+M_B}\sqrt{E_A+M_A}[t(s)]_{BA}. \tag{35}$$

At this point we have to renormalize the divergent integrals appearing in the solution of the BSE. This issue has been carefully discussed in the context of meson-meson scattering (see Sec. 3.4 of Ref. [11]) and applies equally well in the present context. In summary, the result of that discussion amounts to write the renormalized amplitudes (finite) in the same way as the divergent amplitudes but with the previously divergent integrals taken as finite renormalized constants. Ideally one would like to derive them from the underlying QCD dynamics, but in practice it proves easier to fit them to experiment. This amounts to consider, besides the physical masses and weak meson decay constants, 12 fitting parameters that define three diagonal matrices in the coupled channel space which appeared already in the solution of the BSE given, e.g., in Eq. (29). These matrices are

$$J_0[s=(\hat{m}+\hat{M})^2]=\begin{pmatrix} J_{\pi N} & 0 & 0 & 0\\ 0 & J_{\eta N} & 0 & 0\\ 0 & 0 & J_{K\Lambda} & 0\\ 0 & 0 & 0 & J_{K\Sigma}\end{pmatrix},$$
$$\Delta_{\hat{M}}=\begin{pmatrix} \Delta_{N,1} & 0 & 0 & 0\\ 0 & \Delta_{N,2} & 0 & 0\\ 0 & 0 & \Delta_{\Lambda} & 0\\ 0 & 0 & 0 & \Delta_{\Sigma}\end{pmatrix},$$
$$\Delta_{\hat{m}}=\begin{pmatrix} \Delta_{\pi} & 0 & 0 & 0\\ 0 & \Delta_{\eta} & 0 & 0\\ 0 & 0 & \Delta_{K,1} & 0\\ 0 & 0 & 0 & \Delta_{K,2}\end{pmatrix}, \tag{36}$$

where we have denoted the meson-baryon low energy constants $J_0[s=(m_i+M_j)^2]$, $i=\pi,\eta,K,K$, and $j=N,N,\Lambda,\Sigma$ of Eq. (A8) as J_{ij}. The matrix $\Delta_{\hat{m},\hat{M}}$ which appears in Eq. (29) is determined by the matrices $\Delta_{\hat{m}}$ and $\Delta_{\hat{M}}$ above, as it is defined in Eq. (A7). On the other hand, the $\Delta_{K,1}$ and the $\Delta_{K,2}$ matrix elements of the matrix $\Delta_{\hat{m}}$ and the $\Delta_{N,1}$ and the $\Delta_{N,2}$ matrix elements of the matrix $\Delta_{\hat{M}}$ have been taken in general

[11]Despite that and because of the Dirac structure $\not{p}$, the amplitude of Eq. (31) not only contains s-wave, but also a small p-wave.

to be different. This is because, though their formal expression as divergent integrals in Eqs. (A5) and (A7) are the same, after doing the needed renormalization there is no reason why the finite parts in these two channels should coincide.[12]

III. NUMERICAL RESULTS

Throughout the paper we will use the following numerical values for masses and weak decay constants of pseudoescalar mesons (all in MeV),

$$m_\pi = 139.57 \quad m_\eta = 547.45 \quad m_K = 497.67$$

$$M_N = \begin{cases} M_p = 938.27 \\ \\ M_n = 939.57 \end{cases} \qquad M_\Lambda = 1115.68 \quad M_\Sigma = 1192.55$$

$$f_\pi = 93.2 \quad f_\eta = f_K = 1.3 f_\pi \tag{37}$$

where for channel 11 the proton mass is used because the data have been obtained from the $\pi^- p$ scattering, and for channel 22 we take the neutron mass because the available data come from $\pi^- p \to \eta n$. In this way we ensure the exact and physical position of the thresholds. This proves important due to the proximity of the $N(1535)$ to the ηn threshold.

A. Fitting procedure

We perform a χ^2 fit with 12 free parameters considering the following experimental data and conditions.

$S_{11}\pi N$ elastic phase shifts and inelasticities [22], 1077.84 MeV$\leqslant\sqrt{s}\leqslant$1946.52 MeV. In this c.m. energy region, there are a total number of 281 phase shifts and inelasticity data points. Though we have considered four coupled channels, the three-body $\pi\pi N$ channel is not explicitly considered. This omission influences both the phase shifts and the inelasticities and we will assume here that the effect is much more important for the inelasticities than for the phase shifts. Thus, we have fitted the phase shifts while inelasticities have been considered only to impose some constraints on the fit. While $\eta > 0.99$, we have considered that the $\pi\pi N$ channel is essentially closed. In the data, this is the case for c.m. energies below $\sqrt{s} = 1406.4$ MeV. In this energy region, we have assigned to the phase shifts a 3% relative error added in quadrature with a systematic 1° absolute error, in the spirit of Ref. [5]. In this way, we are assuming that any $\pi\pi N$ subthreshold effects are effectively incorporated in the systematic error mentioned above. At higher energies, inelasticities are smaller than 0.99 and we provide the phase shifts with a systematic 15° absolute error added in quadrature with a 3% relative error. The reason for this big systematic error is to account for the explicit omission of the, now open and likely important, three-body channel.

Despite being able to account for a part of the inelasticities (ηN, $K\Lambda$, and $K\Sigma$ channels) and because of the explicit omission of the $\pi\pi N$ channel, inelasticities have not been fitted. Nevertheless, some constraints are imposed in order to prevent the occurrence of smaller inelasticities than the experimental ones. On a quantitative level this means the following. Firstly, we provide the inelasticities with a 3% relative error added in quadrature with 0.01 absolute error. In the second step within the χ^2 fit procedure and given a set of parameters, we compute the theoretical inelasticity for each $\sqrt{s}$. If it turns out that for one c.m. energy the inelasticity is smaller than the experimental value, taking into account the provided errors, we strongly disfavor this set of parameters by decreasing the total error on the inelasticity for this c.m. energy by an order of magnitude when calculating its contribution to the total χ^2. Besides, those energies for which the theoretical inelasticities fall above the experimental ones are set to contribute zero to the total χ^2. In this way, we do not force the fit to pass through the experimental inelasticities at all, but we avoid the unphysical scenario where $\Sigma_{i=\eta N, K\Lambda, K\Sigma} \sigma_i^{\text{theoretical}} > \sigma_{\text{inel}}^{\text{experimental}}$.

Total $\pi^- p \to \eta n$ cross section [23], 1488.4 MeV$\leqslant\sqrt{s}\leqslant$1563.8 MeV. We fit the region close to the ηn threshold and in terms of the commonly used q_{LAB} [incoming pion momentum in the laboratory (LAB) system], the above range corresponds to 687 MeV$\leqslant q_{\text{LAB}} \leqslant$812 MeV. There is a total number of 11 data points. The experimental uncertainties are provided in Ref. [23]. In addition, the experimental cross section has the contribution not only of the *s* wave, the object of this work, but also of the rest of the higher partial waves. Next to threshold the *s* wave is the dominant contribution and the higher energy cut (1563.8 MeV) determines the region up to where it is still a good approximation to the total cross section. For higher energies the *p* wave does play an important role and cannot be neglected, Ref. [4].

We have neglected any possible effect stemming from the $\pi\pi N$ intermediate state in this inelastic channel, as it has been also assumed previously in Refs. [3] and [9].

Total $\pi^- p \to K^0 \Lambda$ cross section [23], 1617.5 MeV$\leqslant\sqrt{s}\leqslant$1724.8 MeV. We fit the region close to the $K^0\Lambda$ threshold, 904 MeV$\leqslant q_{\text{LAB}} \leqslant$1097 MeV with the experimental error bars provided in Ref. [23]. There is a total number of 45 data points and the remarks concerning both the contribution of the $\pi\pi N$ channel and *p* wave effects of the previous item apply also here.

Note that we have not fitted the $\pi^- p \to K^0 \Sigma^0$ total cross section because of the likely sizable isospin 3/2 contribution.

B. Results of the best χ^2 fit

The best fit parameters are compiled in Appendix C. The errors on the parameters turn out to be fairly small. They are purely statistical and have been obtained from the 68% confidence level on the best-fit parameter 12-dimensional distributions. We generate these parameter distributions out of $N = 10^4$ samples. Each of the samples is obtained from a χ^2 fit

[12]This point is clearly exemplified in the $\pi\pi$ BSE treatment, see Eq. (A15) in Ref. [11], where constants which stem from the same divergent integrals, after renormalization, become in fact different functions of the $SU(2)$ low energy constants $\bar{l}$'s.

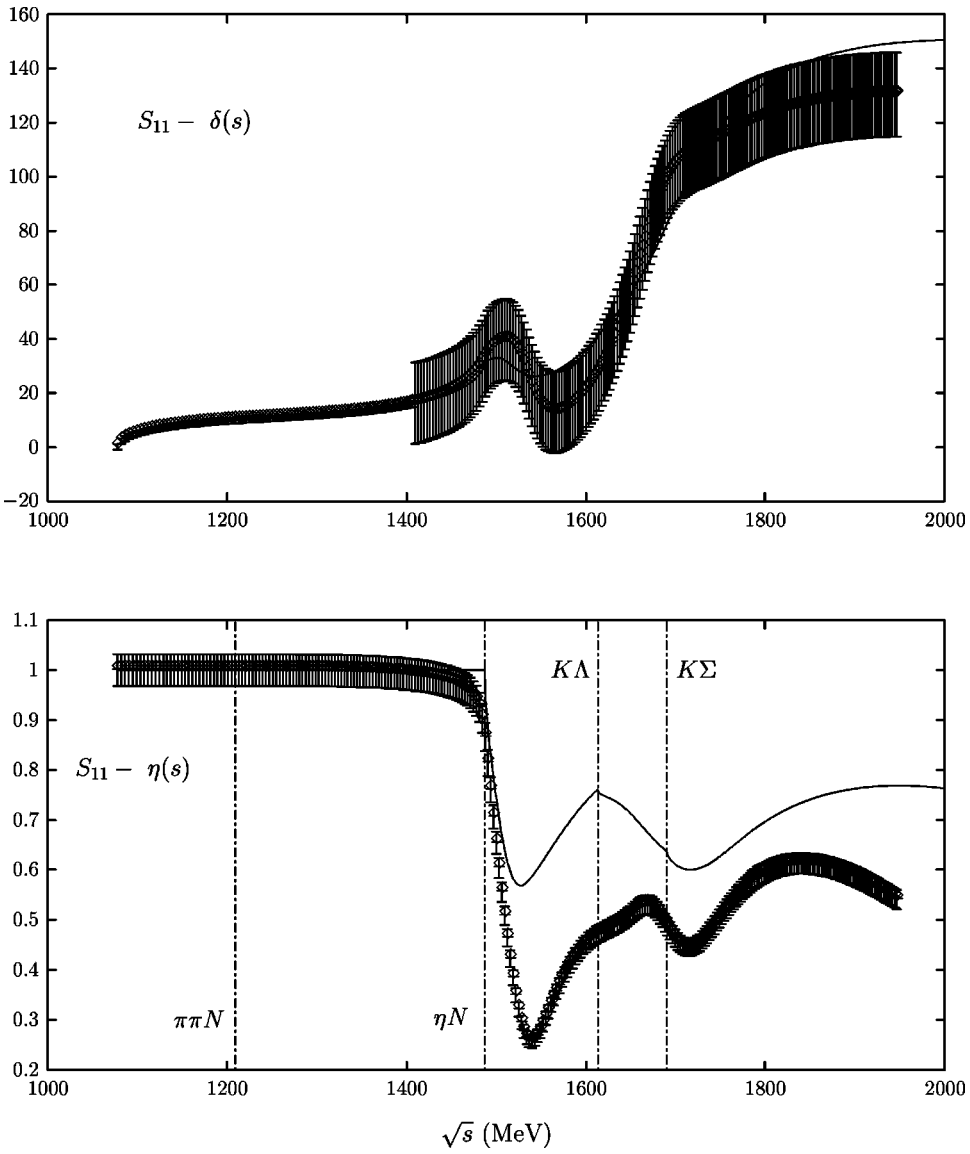

FIG. 2. S_{11}-elastic πN phase shifts and inelasticities as a function of c.m. energy $\sqrt{s}$. Data are from Ref. [22]. Solid lines stand for the lowest-order BSE results with parameters given in Appendix C. Dotted-dashed vertical lines in the bottom plot indicate the energies for which new channels are opened.

to a synthetic set of data points which are obtained from the original one by a Gaussian sampling procedure, i.e., the total number of fits is $N=10^4$. We use the so obtained distributions to evaluate the correlation matrix between the parameters. The correlation matrix is also given in Appendix C. In addition, quantities coming from a χ^2 fit are Gauss distributed in the limit of small errors, as seems to be the case here, therefore the correlation matrix determines the parameter distributions.

Systematic errors on the parameters are not included and they are difficult to estimate. We cannot completely discard that they might be sizable. This situation reflects the present status of the art in unitarized calculations.

In Figs. 2 and 3 we show the results of our approach, with parameters given in Appendix C, for those quantities which have been fitted to. In Fig. 3 only the data for energies below the vertical dotted-dashed lines have been included in the fit. The overall description is remarkably good and that gives us some confidence on the used nonperturbative resummation procedure based on the BSE. For the elastic $\pi N\to\pi N$ scattering length we get

$$a_0^{1/2}\equiv[f_0^{1/2}[s=(m_\pi+M_N)^2]]_{\pi N\leftarrow\pi N}=0.179\pm0.004\ \text{fm}, \tag{38}$$

where the error is statistical and it has been obtained from those in the best fit parameters [Eq. (C1)], taking into account the existing statistical correlations, through a Monte Carlo simulation. This value should be compared both to the recent experimental one 0.252 ± 0.006 fm of Ref. [24] and to the HBChPT result to third order of Ref. [14] 0.19 ± 0.05 fm. The agreement between our coupled channel unitarized scattering length with that from NNLO-HBChPT is satisfactory from a theoretical viewpoint since in both cases the same set of low energy data [22] have been used. The discrepancy of our number with the experimental one of Ref. [24] possibly points toward a too conservative error assignment of the low energy phase-shifts in Ref. [22].

In principle, the LEC's of Eq. (C1) determine, or vice versa they can be determined from, the next-to-leading order results of ChPT, as is explicitly shown in Ref. [11], for the case of elastic $\pi\pi$ scattering. However, the perturbative calculation is not available and it only exists next-to-leading

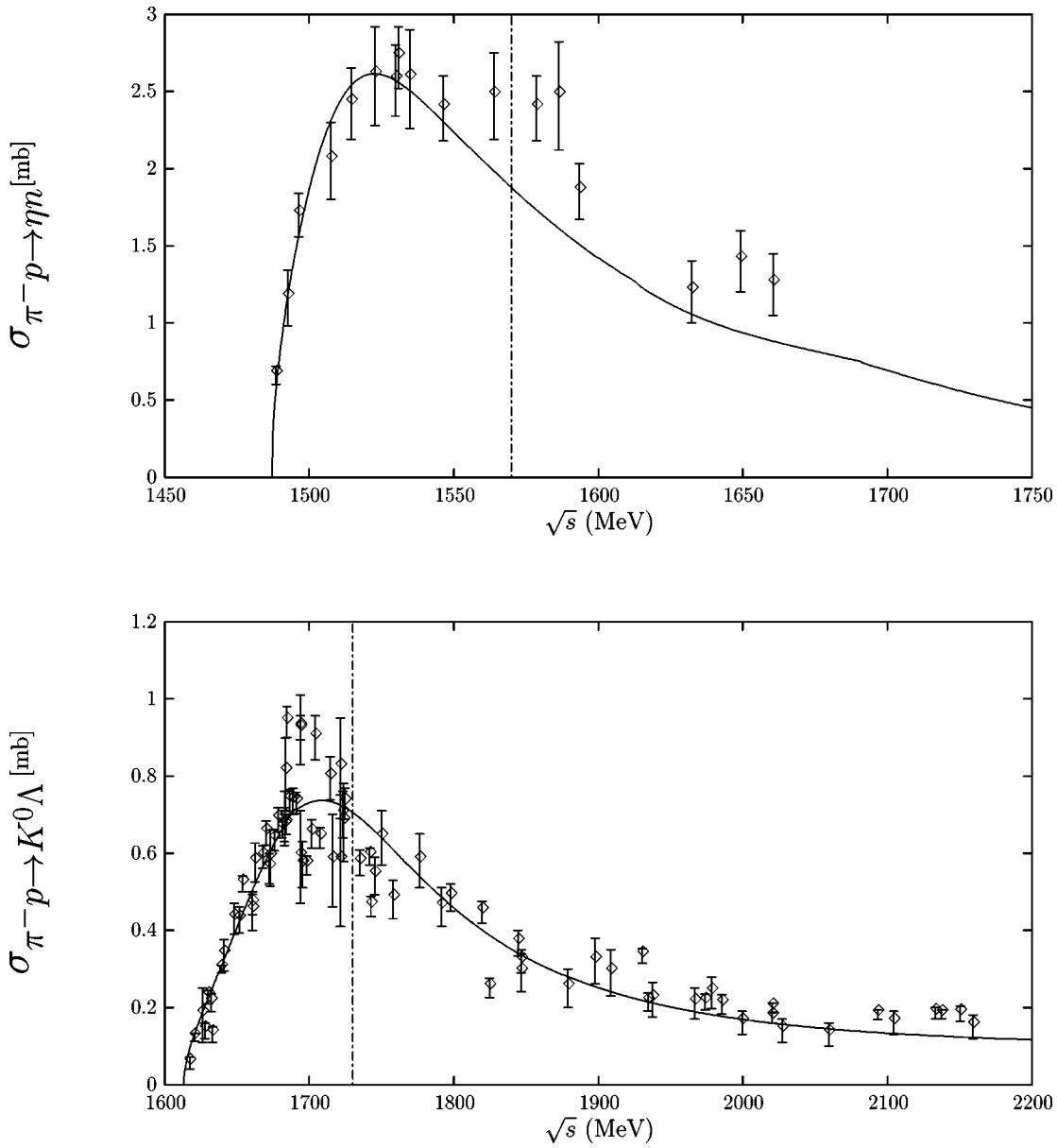

FIG. 3. Total $\pi^- p\to\eta n$ and $\pi^- p\to K^0\Lambda$ cross sections as a function of the c.m. energy. Data are from Ref. [23]. Solid lines stand for the lowest-order BSE S_{11} results with parameters given in Appendix C. Data for energies above the vertical dotted-dashed lines have not been included in the fit.

results for πN, with no coupled channels [5,17,25,26], in the framework of heavy baryon chiral perturbation theory (HBChPT). In Appendix D we discuss this point in more detail.

C. Predictions for other processes

In Fig. 4 we show some of our predictions for phase shifts, inelasticities and s-wave $T=1/2$ partial cross sections for some other channels. For most of them there are no data. The $\eta N\to\eta N$ elastic phase shifts (top left panel) present a steep raise close to the threshold going up to $70°$, which corresponds to a typical low energy resonance behavior triggered by the $N(1535)$ resonance (see the next section). Accordingly, the corresponding partial cross section (bottom panel) takes an unnaturally large value as compared to other elastic and transition cross sections. This is in contrast to any expectation based in the Born approximation, since the corresponding potential in this channel vanishes [see Eq. (8)].

The effect of the $N(1535)$ can also be seen at the figure (bottom panel) by the maximum in $\pi N\to\eta N$ cross section and the cusp effect in the $\pi N\to\pi N$ partial cross section. On the other hand, $K\Lambda\to K\Lambda$ phase shifts (top right panel) turn out to be extremely small. The effect of the $N(1650)$ can also be seen at the cross sections, particularly in the $\pi N\to\pi N$ partial cross section, though the effect is less pronounced than in the $N(1535)$ case. We have not plotted the elastic $K\Sigma\to K\Sigma$ cross section since the physical process involves also the isospin $T=3/2$ channel, not considered in this work.

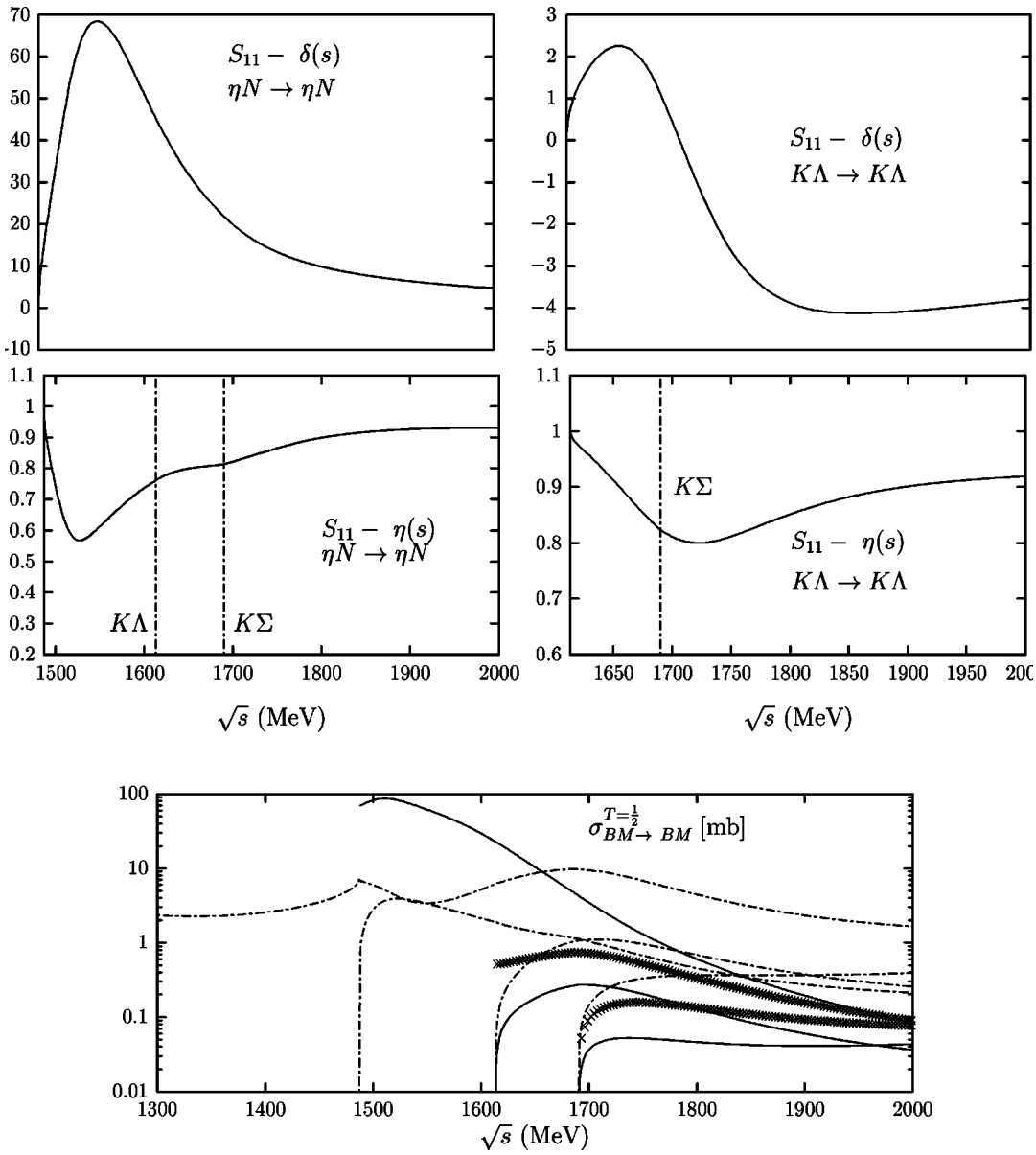

FIG. 4. Top panel: s-wave $T=1/2$ phase shifts (in degrees) for elastic $\eta N \to \eta N$ (left panel) and $K\Lambda \to K\Lambda$ (right panel) processes as functions of the c.m. energy. Middle panel: same as before but for inelasticities. Vertical lines indicate the opening of reaction thresholds. Bottom panel: s-wave $T=1/2$ meson-baryon cross sections ($\pi N \to \pi N, \eta N, K\Lambda, K\Sigma$; $\eta N \to \eta N, K\Lambda, K\Sigma$; $K\Lambda \to K\Lambda, K\Sigma$) in mbarns as functions of the c.m. energy. Dashed lines indicate the πN initial state. Solid lines indicate the ηN initial state. Crosses indicate the $K\Lambda$ initial state. All the lines start at the relevant final state threshold (with the exception of the elastic $\pi N \to \pi N$ reaction).

Our estimates for ηN and $K\Lambda$ scattering lengths (defined for the elastic channels) similarly as in Eq. (38) are

$$a_{\eta N} = 0.772(5) + \mathrm{i}\, 0.217(3)\ \mathrm{fm},$$

$$a_{K\Lambda} = 0.0547(5) + \mathrm{i}\, 0.032(4)\ \mathrm{fm}, \qquad (39)$$

respectively. The scattering length $a_{\eta N}$ compares reasonably well with the one obtained in Ref. [3], $a_{\eta N} = 0.68 + \mathrm{i}\, 0.24$ fm.

D. Second Riemann sheet: Poles and resonances

In this section we are interested in describing masses and widths of the S_{11} resonances. An illustrative picture of the complex c.m. energy plane with the singularities from the Particle Data Book [27] is presented in Fig. 5. For a more distinctive characterization of the resonances one has to look for poles in the complex s plane.

Since causality imposes the absence of poles in the physical sheet [28], one should search for complex poles in unphysical ones. Among all of them, those *closest* to the physical sheet are the most relevant ones. For the sake of clarity, we will devote some space here to explain, in a quantitative manner, the meaning of ''close'' in this context. We look for poles in the coupled channel matrix amplitude $t(s)$ defined in Eq. (33). We have only examined the entry 11, $\pi N \to \pi N$, of that matrix. The position of the complex poles, as long as they are produced for physical resonances, should be

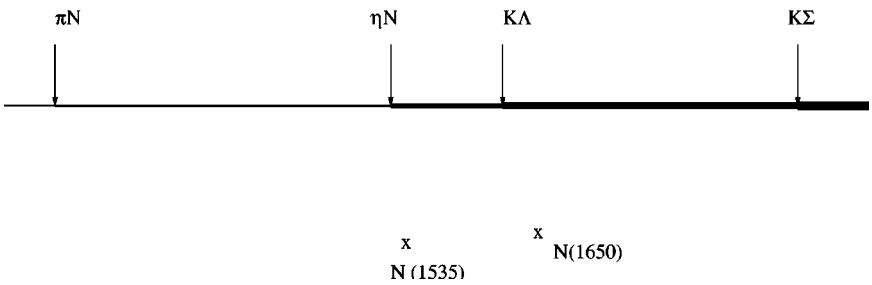

FIG. 5. Location of reaction thresholds and resonances in the complex c.m. energy plane. The corresponding unitarity cuts have increasing thickness for increasing energy.

independent of the particular channel. However, residues at the pole do depend on the examined channel because they determine the coupling of each of the channels to the resonances. This interesting point will be discussed elsewhere [29].

To begin with, let us assume a situation where the coupled channel formalism is not needed, i.e., an artificial situation where only the 11 element of the first column and row of the D matrix in Eq. (8) is nonvanishing. In such a case, elastic unitarity requires only a unique finite branch point at $s=s_+=(M_N+m_\pi)^2$ and a cut along the line $[s_+,+\infty[$. The scattering amplitude in the unphysical second Riemann sheet $[t_{II}(s)]$ is simply obtained by analytical continuation of the amplitude in the physical first Riemann sheet $[t(s)\equiv t_I(s)]$ across the unitarity cut, and therefore the following relation for inverse amplitudes should hold (s real and above s_+):

$$t_{II}^{-1}(s+\mathrm{i}\,\epsilon)=t_I^{-1}(s-\mathrm{i}\,\epsilon). \tag{40}$$

The unitarity condition for the inverse amplitude, deduced from Eqs. (33), (30), and (A12) reads

$$\mathrm{Disc}[t^{-1}(s)]\equiv t_I^{-1}(s+\mathrm{i}\,\epsilon)-t_I^{-1}(s-\mathrm{i}\,\epsilon)=2\,\mathrm{i}\,\rho(s),\quad s>s_+ \tag{41}$$

with $s\in\mathbb{R}$, where the phase-space function

$$\rho(s)=\frac{\lambda^{1/2}(s,m_\pi,M_N)}{16\pi s}\times\frac{(\sqrt{s}+M_N)^2-m_\pi^2}{2\sqrt{s}} \tag{42}$$

has been introduced, understanding that $\rho(s)$ is a function of the real variable s. Then, analytically continuing the phase-space function to all complex planes, the unitarity condition reads

$$t_I^{-1}(s+\mathrm{i}\,\epsilon)-t_I^{-1}(s-\mathrm{i}\,\epsilon)=2\,\mathrm{i}\,\rho(s+\mathrm{i}\,\epsilon),\quad s_+<s\in\mathbb{R} \tag{43}$$

where the cuts for $\lambda^{1/2}(z,m_\pi^2,M_N^2)$ go along the real axis for $-\infty<s<s_-$ and $s_+<s<\infty$. The function is chosen to be real and positive on the upper lip of the second cut, $s_+<s<\infty$ and hence it satisfies:

$$\lambda^{1/2}(s+\mathrm{i}\,\epsilon,m_\pi^2,M_N^2)=-\lambda^{1/2}(s-\mathrm{i}\,\epsilon,m_\pi^2,M_N^2)=|\lambda^{1/2}(s,m_\pi^2,M_N^2)|,\quad s_+<s\in\mathbb{R}. \tag{44}$$

Besides, the cut for the $\sqrt{z}$ function, also appearing in $\rho(z)$, is taken along the line $]-\infty,0]$ and the multivalued function

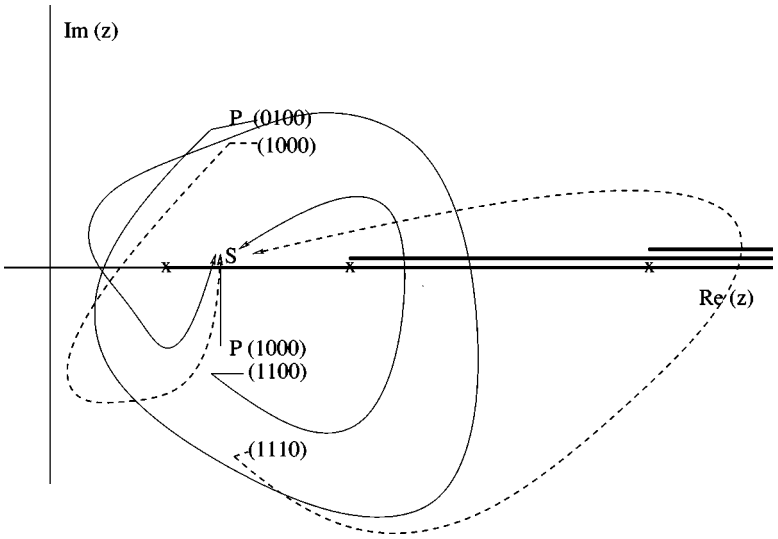

FIG. 6. Different paths in the s complex plane showing how to reach the point S located in the physical scattering region in the interval $[(m_\pi+M_N)^2,(m_\eta+M_N)^2]$ from points P (eventually poles) located in different Riemann sheets, denoted by the vector **n** as introduced in Eq. (48), and placed both in the first and fourth quadrants. The unitarity cuts are also depicted in the figure. The ''distance'' between S and P is obtained by the length of the shortest path joining them. This can be achieved after continuous deformation of the paths depicted in the figure, i.e., any deformations without intersecting the branch points.

is taken to be positive for real and positive values of z. Now using Eqs. (40) and (43) one finds the amplitude in the second Riemann sheet,

$$t_{II}^{-1}(z)=t_I^{-1}(z)-2\,\mathrm{i}\,\rho(z),\quad z\in\mathbb{C}. \tag{45}$$

On the other hand,

$$\begin{aligned} t_{II}^{-1}(s-\mathrm{i}\,\epsilon)&=t_I^{-1}(s-\mathrm{i}\,\epsilon)-2\,\mathrm{i}\,\rho(s-\mathrm{i}\,\epsilon)=t_I^{-1}(s+\mathrm{i}\,\epsilon)\\ &\quad-2\,\mathrm{i}\,\rho(s+\mathrm{i}\,\epsilon)-2\,\mathrm{i}\,\rho(s-\mathrm{i}\,\epsilon)\\ &=t_I^{-1}(s+\mathrm{i}\,\epsilon),\quad s_+<s\in\mathbb{R} \end{aligned} \tag{46}$$

which means that there are only two Riemann sheets linked to the unitarity cut. The analytical structure, concerning the unitarity cut, of the inverse amplitude is determined by the function

$$-\overline{J}_0(s)\times\left(\frac{s-m_\pi^2+M_N^2}{2\sqrt{s}}+M_N\right) \tag{47}$$

as it is deduced from Eqs. (33), (30), and (A8). Because of the choice of cuts for the multivalued function $\sqrt{z}$ above, the function $L(s)$ introduced in Eq. (A9) determines the analytical structure of $t(s)$. Thus, the two Riemann sheets of $t(s)$ related to the unitarity cut are obtained from the values $n=0$ and 1 in Eq. (A13) for $L(z,n)$.

In the general case of multiple thresholds, as is the case in this work, the above conclusions hold for any of the finite branch points, located at the physical thresholds, and unitarity related cuts going along the lines [branch point, ∞[.

For four channels there are a total number of $2^4=16$ Riemann sheets related to unitarity. Now, $\overline{J}_0(s)$ and hence $L(s)$ become diagonal matrices in the coupled channel space: namely,

$$\mathbf{L}(z,\mathbf{n})=\begin{pmatrix} L_{m_\pi M_N}(z,n_{\pi N}) & 0 & 0 & 0\\ 0 & L_{m_\eta M_N}(z,n_{\eta N}) & 0 & 0\\ 0 & 0 & L_{m_K M_\Lambda}(z,n_{K\Lambda}) & 0\\ 0 & 0 & 0 & L_{m_K M_\Sigma}(z,n_{K\Sigma}) \end{pmatrix} \tag{48}$$

with $z\in\mathbb{C}$, $\mathbf{n}=(n_{\pi N},n_{\eta N},n_{K\Lambda},n_{K\Sigma})$ and the dependence in the masses of the function L is explicitly given. The first Riemann sheet $[t_I(s)]$ corresponds to the choice $\mathbf{n}=(0,0,0,0)$. As mentioned above, poles can only occur in any of the remaining 15 Riemann sheets. The closer the position of the pole to the scattering region (the upper lip of the first Riemann sheet) the bigger is the influence on the scattering amplitude. All Riemann sheets can be reached continuously from the first one by looping around the appropriate branch points. From this point of view, close means proximity following a continuous path. Thus, for the region $(m_\pi+M_N)^2<s<(m_\eta+M_N)^2$ the poles of the (1,0,0,0) Riemann sheet, located in the fourth quadrant and with values of Rez belonging to the above interval, are expected to have the biggest influence on the scattering amplitude, as is illustrated in Fig. 6. Similarly, for the region $(m_\eta+M_N)^2<s<(m_K+M_\Lambda)^2$ the poles of the (1,1,0,0) Riemann sheet, located in the fourth quadrant and with values of Re$\,z$ belonging to the above interval, are expected to play a crucial role, and so on $\ldots$.

Thus, we define the ''second Riemann sheet'' in the relevant fourth quadrant $[t_{II}(s)]$ as that which is obtained by continuity across each of the four unitarity cuts. It is obtained using for the diagonal matrix $\overline{J}_0(s)$ the following function:[13]

$$\mathcal{L}_{II}(z)=\begin{cases} \mathbf{L}(z;1,0,0,0) & \text{if } (m_\pi+M_N)^2<\mathrm{Re}(z)<(m_\eta+M_N)^2\\ \mathbf{L}(z;1,1,0,0) & \text{if } (m_\eta+M_N)^2<\mathrm{Re}(z)<(m_K+M_\Lambda)^2\\ \mathbf{L}(z;1,1,1,0) & \text{if } (m_K+M_\Lambda)^2<\mathrm{Re}(z)<(m_K+M_\Sigma)^2\\ \mathbf{L}(z;1,1,1,1) & \text{if } (m_K+M_\Sigma)^2<\mathrm{Re}(z). \end{cases} \tag{49}$$

[13]Though each of the functions $\mathbf{L}(z;\mathbf{n})$ are analytical in the complex plane, except for the pertinent unitarity cuts, note that $\mathcal{L}_{II}$ so defined is continuous for real values of s, but presents additional discontinuities out of the real axis.

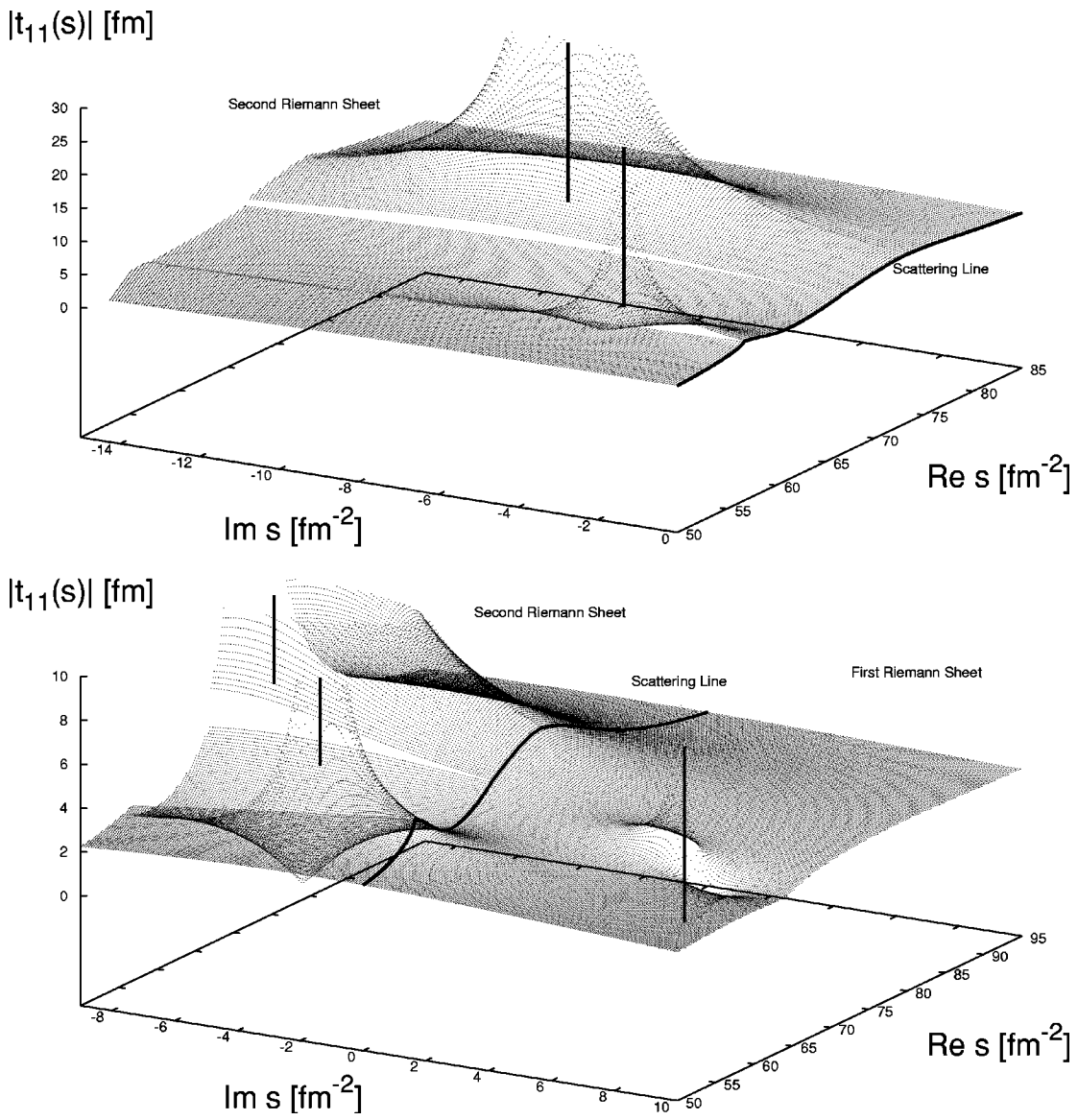

FIG. 7. Modulus of the $\pi N \to \pi N$ element of the scattering amplitude $t(s)$, defined in Eq. (33), in the s-complex plane. In both plots, vertical lines indicate the position of the poles. Top panel: Fourth quadrant of the ''second Riemann sheet,'' as defined in Eq. (49), and the physical scattering line. The two observed poles are identified to be the $S_{11}-N(1535)$ and $-N(1650)$ resonances as it is discussed in the main text. Bottom panel: Fourth quadrant of the ''second Riemann sheet'' and the first quadrant of the first (physical) Riemann sheet. Besides the two poles already appearing in the top panel, there is a third one. Though it is unphysical because it appears in the physical sheet out of the real axis, it does not influence the scattering line as the plot clearly shows.

In Fig. 7 we show the absolute value of the $t_{11}(s)$ element of the scattering amplitude both for the fourth quadrant of the ''second Riemann sheet'' and the first quadrant of the first (physical) Riemann sheet. The physical scattering takes place in the scattering line in the plots (upper lip of unitarity cut of the first Riemann sheet). The positions of the two poles in the ''second Riemann sheet'' are ($s=M_R^2 - \mathrm{i}\, M_R \Gamma_R$):

$$\text{first pole:} \quad M_R = 1496.5 \pm 0.4, \quad \Gamma_R = 83.3 \pm 0.7, \tag{50}$$

$$\text{second pole:} \quad M_R = 1684.3 \pm 0.7, \quad \Gamma_R = 194.3 \pm 0.8, \tag{51}$$

where all units are given in MeV and errors have been transported from those in the best fit parameters [Eq. (C1)], taking into account the existing statistical correlations, through a Monte Carlo simulation. These poles are resonances and can be identified to be the $S_{11}-N(1535)$ and $-N(1650)$ ones which, according to Ref. [27] [Particle Data Group (PDG)], are located at

$$N(1535): \quad M_R = 1505 \pm 10, \quad \Gamma_R = 170 \pm 80, \tag{52}$$

$$N(1650): \quad M_R = 1660 \pm 20, \quad \Gamma_R = 160 \pm 10, \tag{53}$$

where again units are in MeV and we quote data from the position of the poles which are slightly different to those

deduced from a Breit-Wigner fit. The agreement of our predictions and the PDG ones is satisfactory. Our calculated width for the $N(1535)/N(1650)$ turns out to be smaller/larger than the experimental one, in great part because its mass is slightly smaller/larger than the data and hence the available phase space for the decay decreases/increases. Besides, the inclusion of the three-body channel ($\pi\pi N$) would influence both the widths and the masses of the resonances.

Residues at the poles depend on the examined channel, because they determine the coupling of each of the channels to the resonances. Thus, from the results shown in Fig. 7 one could predict the coupling of the $N(1535)$ and $N(1650)$ resonances to πN. A detailed study of the couplings of these resonances to all channels, not only πN, is presently under way.

On the other hand, there is a unphysical pole in the physical (first) Riemann sheet. It is located at $(s=M^2+\mathrm{i}M\Gamma)M \approx 1582$ MeV and $\Gamma \approx 166$ MeV and it violates the Mandelstam's hypothesis of maximal analyticity [28]. This unphysical pole appears because we have truncated the iterated potential to solve the BSE. However, as can be seen in the plots, the two poles in the ''second Riemann sheet'' have a much larger influence on the physical scattering than the spurious (unphysical) one. Thus, the influence of this unphysical pole may be disregarded.[14]

IV. CONCLUSIONS

In this paper we have developed a Bethe-Salpeter formalism to study s-wave and $T=1/2$ meson-baryon scattering up to almost 2 GeV. We work on a four-dimensional two-body channel space and the kernel of the BSE takes into account chiral symmetry constraints as deduced from the corresponding effective Lagrangian. At lowest order in the chiral expansion for the potential, an analytical explicit solution is found which manifestly complies with multiple channel unitarity. Among the several issues which can be explored using the present formalism, we have focused our attention on πN elastic scattering (phase shifts and inelasticities) and the measured inelastic cross sections, the agreement with experiment being rather good. Besides, some predictions for other cross sections, not yet measured, have also been given. We have undertaken a careful discussion on the analytical structure and continuation of the scattering matrix amplitude to the complex s-plane, which becomes mandatory in order to extract the location of the S_{11} resonances. We have searched for poles in the ''second Riemann sheet'' and compared both masses and widths to data. The agreement is also quite satisfactory. Thus, and despite having neglected the three-body production channel $\pi\pi N$, we provide a rather successful description of the s-wave and $T=1/2$ meson (π,η,K)-baryon $(\mathrm{N},\ \Lambda,\ \Sigma)$ scattering up to almost 2 GeV in the strangeness zero channel. Couplings of the $N(1535)$ and $N(1650)$ resonances to the different open meson-baryon channels can be obtained from our amplitudes and it will be discussed elsewhere.

Nevertheless our calculation has some obvious limitations and hence it might be improved. Besides the inclusion of the $\pi\pi N$ channel,[15] one should consider the inclusion of higher-order terms in the two-particle irreducible matrix amplitude (potential) which would lead to a realistic predictions for higher partial waves in the $T=1/2$ channel. Understanding the free parameters of our model and their numerical values presented in Eq. (C1), in terms of the LEC's appearing in the higher chiral Lagrangian order pieces, either within the HBChPT formalism [17] or in the fully covariant framework recently developed in Ref. [30], would be obviously desirable. As we have shown in Appendix D, such a task would, at least, require to know the perturbative $1/f^6$ order to take into account the likely important ηN-channel effects, which are effectively incorporated in the BSE scheme presented in this work.

Given the phenomenological success of the presented framework, it seems natural to extend it to other nonzero strangeness channels; for a recent overview of related aspects see for instance Ref. [31], or to the study of meson photoproduction processes.

ACKNOWLEDGMENTS

We warmly thank C. Garcia-Recio, E. Oset, A. Parreño, J.R. Peláez, and A. Ramos for useful discussions. This research was supported by DGES under contract PB98-1367 and by the Junta de Andalucia.

APPENDIX A: BASIC INTEGRALS

We display the explicit expressions for the loop integrals used in this paper. The basic integrals appearing in the solution of the BSE are

$$J(\not P)=\mathrm{i}\int\frac{d^4q}{(2\pi)^4}\frac{1}{q^2-\hat m^2}\frac{1}{\not P-\not q-\hat M}, \tag{A1}$$

$$J_1^R(\not P)=\mathrm{i}\int\frac{d^4q}{(2\pi)^4}\frac{1}{q^2-\hat m^2}\frac{1}{\not P-\not q-\hat M}\not q$$
$$=J(\not P)(\not P-\hat M)-\Delta_{\hat m}, \tag{A2}$$

[14]Because of Schwartz's reflection principle there is also a pole in the fourth quadrant of the first Riemann sheet (complex conjugated of that given above) whose influence is even more negligible than that of the first quadrant. This is because it is placed at a substantially larger distance of the upper lip of the unitarity cut. The existence of other complex conjugated poles, both in the first Riemann sheet or in any of the unphysical sheets, is not precluded, but from Fig. 7 we infer that their influence in the scattering is not significant.

[15]In our point of view, it is a highly nontrivial task to find a solution of the BSE including a three-body intermediate state exactly complying to three-body unitarity. In some cases, for instance for elastic $\pi N\to\pi N$, meson η production, ..., some insight might be obtained by treating perturbatively the process, as our results suggest.

$$J_1^L(\not p)=\mathrm{i}\int\frac{d^4q}{(2\pi)^4}\frac{1}{q^2-\hat m^2}\not q\frac{1}{\not p-\not q-\hat M}$$
$$=(\not p-\hat M)J(\not p)-\Delta_{\hat m}, \tag{A3}$$

$$J_2(\not p)=\mathrm{i}\int\frac{d^4q}{(2\pi)^4}\frac{1}{q^2-\hat m^2}\not q\frac{1}{\not p-\not q-\hat M}\not q$$
$$=(\not p-\hat M)J(\not p)(\not p-\hat M)-(\not p-\hat M)\Delta_{\hat m} \tag{A4}$$

and the results are obtained from relativistic and translational invariance requirement in momentum space. Here, $\Delta_{\hat m}$ is a quadratically divergent integral

$$\Delta_{\hat m}=\mathrm{i}\int\frac{d^4q}{(2\pi)^4}\frac{1}{q^2-\hat m^2}, \tag{A5}$$

which would require renormalization. Besides, the linearly divergent integral $J(\not p)$ can be evaluated yielding

$$J(\not p)=\not p\left[\left(\frac{s-\hat m^2+\hat M^2}{2s}\right)J_0(s)+\frac{\Delta_{\hat m\hat M}}{2s}\right]+\hat M J_0(s), \tag{A6}$$

$$\Delta_{\hat m\hat M}=\Delta_{\hat m}-\Delta_{\hat M}=\mathrm{i}\int\frac{d^4q}{(2\pi)^4}\frac{1}{q^2-\hat m^2}-\mathrm{i}\int\frac{d^4q}{(2\pi)^4}\frac{1}{q^2-\hat M^2}, \tag{A7}$$

where $\Delta_{\hat m\hat M}$ is quadratically divergent as well and the logarithmically divergent integral $J_0(s)$ needs one subtraction to make it finite. Choosing for definiteness the threshold value $s=(\hat m+\hat M)^2$ we get

$$J_0(s)=\mathrm{i}\int\frac{d^4q}{(2\pi)^4}\frac{1}{q^2-\hat m^2}\frac{1}{(P-q)^2-\hat M^2}$$
$$=\overline{J}_0(s)+J_0[s=(\hat m+\hat M)^2] \tag{A8}$$

with $J_0[s=(\hat m+\hat M)^2]$ a divergent integral and the finite function $\overline{J}_0(s)$ is given by[16]

$$\overline{J}_0(s)=\frac{1}{(4\pi)^2}\left\{\left[\frac{M^2-m^2}{s}-\frac{M-m}{M+m}\right]\ln\frac{M}{m}+L(s)\right\} \tag{A9}$$

and for real s and above threshold, $(m+M)^2$, we have

$$L(s)\equiv L(s+\mathrm{i}\,\epsilon)=\frac{\lambda^{1/2}(s,m^2,M^2)}{s}$$
$$\times\left\{\log\left[\frac{1+\sqrt{\dfrac{s-s_+}{s-s_-}}}{1-\sqrt{\dfrac{s-s_+}{s-s_-}}}\right]-i\pi\right\}, \tag{A10}$$

where we have defined the pseudothreshold and threshold variables as

$$s_-=(m-M)^2,\quad s_+=(m+M)^2, \tag{A11}$$

respectively, and the logarithm is taken to be real. Note that $L(s_+)=0$. For $s>s_+$ the imaginary part along the unitarity cut may be computed directly from the above Eq. (A10) or through Cutkosky's rules,

$$2\,\mathrm{i}\,\mathrm{Im}\,J_0(s)=\mathrm{Disc}J_0(s)=[J_0(s+\mathrm{i}\,\epsilon)-J_0(s-\mathrm{i}\,\epsilon)]$$
$$=\mathrm{i}\int\frac{d^4q}{(2\pi)^2}(-2\pi\,\mathrm{i})^2\delta^+(q^2-m^2)$$
$$\times\delta^+[(P-q)^2-m^2]$$
$$=-2\,\mathrm{i}\frac{\lambda^{1/2}(s,m^2,M^2)}{16\pi s}\Theta(s-s_+). \tag{A12}$$

Up to a $16\pi^2$ factor the function $L(s)$ has the same discontinuity as the function $J_0(s)$. Taking into account that we have to evaluate the function $J_0(s)$ not only for real $s>s_+$ but also below threshold[17] and in the second Riemann sheet as well, to look for the position of resonances in the complex s plane, we give here the analytical continuation of $L(z)$ used in our calculation. Defining $\rho_\pm=|z-s_\pm|$ and taking the principal arguments, Arg(. . .), $\theta_\pm$ of $|z-s_\pm|$ to lie in the range $0\leqslant\theta_+<2\pi$ and $-\pi\leqslant\theta_-<\pi$, respectively, we have

$$L(z,n)=\frac{(\rho_+\rho_-)^{1/2}}{z}e^{\mathrm{i}(\theta_++\theta_-+2n\pi)/2}\{\ln|R(z)|+\mathrm{i}\,\mathrm{Arg}[R(z)]$$
$$-2\pi\,\mathrm{i}\},$$

$$R(z)=\frac{\rho_+^{1/2}e^{\mathrm{i}\,\theta_+/2}+\rho_-^{1/2}e^{\mathrm{i}\,\theta_-/2}e^{\mathrm{i}\,n\pi}}{\rho_+^{1/2}e^{\mathrm{i}\,\theta_+/2}-\rho_-^{1/2}e^{\mathrm{i}\,\theta_-/2}e^{\mathrm{i}\,n\pi}}, \tag{A13}$$

where $\mathrm{Arg}[R(z)]$ should be taken in the interval $[0,2\pi[$. For $n=0$ one gets the first Riemann sheet $L_I(z)=L(z,n=0)$, which only has a (unitarity) cut along the real axis $s_+\leqslant s<\infty$. When going across the unitarity cut once we jump into the second Riemann sheet, corresponding to $n=1$, $L_{II}(z)=L(z,n=1)$. If we loop twice around the threshold branch

[16] $J_0(s)$ is a diagonal matrix in the coupled channel space and for simplicity we work from now on in a given channel.

[17] For instance, when calculating the elastic πN scattering, obviously there are values of s below heavier thresholds ηN, $K\Lambda$, $K\Sigma$.

point $z=s_+$ we come back to the original Riemann sheet. The second Riemann sheet has an additional cut along the real axis $-\infty<s<s_-$ and the following relation holds:

$$L_{II}(z)=L_I(z)+2\pi\,\mathrm{i}\,\frac{\lambda^{1/2}(z,m^2,M^2)}{z}, \tag{A14}$$

where the cuts for $\lambda^{1/2}(z,m^2,M^2)$ go along the real axis for $-\infty<s<s_-$ and $s_+<s<\infty$. The function is chosen to be real and positive on the upper lip of the second cut, $s_+<s<\infty$ and corresponds $|\lambda^{1/2}(s,m^2,M^2)|\equiv\lambda^{1/2}(s+\mathrm{i}\,\epsilon,m^2,M^2)$. The $-2\pi\mathrm{i}$ constant appearing in Eq. (A13) determines the chosen Riemann sheet of the logarithm and ensures that $L_I(z)$ is purely real along the real axis below threshold. Note that since $R(z)$ only vanishes at infinity we never have a chance to cross the cut of the logarithm and never change log-Riemann sheets.

APPENDIX B: DERIVATION OF THE SOLUTION OF THE BSE

Here we show how to derive Eq. (28) displayed in the main text. The ansatz of Eq. (26) reduces the BSE integral equation Eq. (20) into a set of linear equations for the matrix coefficients a, b_R, b_L, and c

$$\begin{aligned}
a&=a[(\not p-\hat M)J-\Delta_{\hat m}]\frac{D}{f^2}+b_L(\not p-\hat M)[(\not p-\hat M)J-\Delta_{\hat m}]\frac{D}{f^2},\\
b_R&=b_R[(\not p-\hat M)J-\Delta_{\hat m}]\frac{D}{f^2}+c(\not p-\hat M)[(\not p-\hat M)J-\Delta_{\hat m}]\frac{D}{f^2}\\
&\quad+\frac{D}{f^2},\\
b_L&=aJ\frac{D}{f^2}+b_L[(\not p-\hat M)J-\Delta_{\hat m}]\frac{D}{f^2}+\frac{D}{f^2},\\
c&=b_RJ\frac{D}{f^2}+c[(\not p-\hat M)J-\Delta_{\hat m}]\frac{D}{f^2}.
\end{aligned} \tag{B1}$$

In the above equation J stands for $J(\not p)$ defined and evaluated in Appendix A. The solution of this matrix system is tricky although straightforward. The main complication arises from the noncommuting character of the fermion mass matrix $\hat M$ with the coupled channel matrices a, b_L, b_R, c, and D. Defining

$$\begin{aligned}
&X=a,\quad Y_R=(\not p-\hat M)b_R,\quad Y_L=b_L(\not p-\hat M),\\
&Z=(\not p-\hat M)c(\not p-\hat M),\quad G=\frac{1}{f^2}[(\not p-\hat M)J-\Delta_{\hat m}].
\end{aligned} \tag{B2}$$

The set of matrix equations can be written as

$$X=XGD+Y_LGD, \tag{B3}$$

$$Y_R=Y_RGD+ZGD+\frac{(\not p-\hat M)D}{f^2}, \tag{B4}$$

$$\begin{aligned}
Y_L=X\left(G+\frac{\Delta_{\hat m}}{f^2}\right)\frac{1}{\not p-\hat M}D(\not p-\hat M)+Y_LG\frac{1}{\not p-\hat M}\\
\times D(\not p-\hat M)+\frac{D(\not p-\hat M)}{f^2},
\end{aligned} \tag{B5}$$

$$\begin{aligned}
Z=Y_R\left(G+\frac{\Delta_{\hat m}}{f^2}\right)\frac{1}{\not p-\hat M}D(\not p-\hat M)+ZG\frac{1}{\not p-\hat M}\\
\times D(\not p-\hat M).
\end{aligned} \tag{B6}$$

Summing Eqs. (B3) and (B4), and Eqs. (B5) and (B6), we get after some matrix reshuffling

$$\frac{(\not p-\hat M)}{f^2}=(X+Y_R)(D^{-1}-G)-(Y_L+Z)G, \tag{B7}$$

$$\begin{aligned}
-\frac{(\not p-\hat M)}{f^2}&=(X+Y_R)\left(G+\frac{\Delta_{\hat m}}{f^2}\right)-(Y_L+Z)\\
&\quad\times[(\not p-\hat M)^{-1}D^{-1}(\not p-\hat M)-G].
\end{aligned} \tag{B8}$$

Subtracting and summing Eqs. (B7) and (B8) we get

$$\begin{aligned}
(X+Y_R)=(Y_L+Z)\Bigg[&(\not p-\hat M)^{-1}D^{-1}(\not p-\hat M)\\
&\times\left(D^{-1}+\frac{\Delta_{\hat m}}{f^2}\right)^{-1}\Bigg],
\end{aligned} \tag{B9}$$

$$\begin{aligned}
\frac{2(\not p-\hat M)}{f^2}&=(X+Y_R)\left(D^{-1}-2G-\frac{\Delta_{\hat m}}{f^2}\right)+(Y_L+Z)\\
&\quad\times[(\not p-\hat M)^{-1}D^{-1}(\not p-\hat M)-2G],
\end{aligned} \tag{B10}$$

respectively. We can then solve for $Z+Y_L$ from Eqs. (B9) and (B10) yielding

$$\begin{aligned}
(Y_L+Z)^{-1}=\Bigg\{\Bigg[&(\not p-\hat M)^{-1}D^{-1}(\not p-\hat M)\\
&\times\left(D^{-1}+\frac{\Delta_{\hat m}}{f^2}\right)^{-1}+1\Bigg](-2G)+(\not p-\hat M)^{-1}\\
&\times D^{-1}(\not p-\hat M)\Bigg[\left(D^{-1}+\frac{\Delta_{\hat m}}{f^2}\right)^{-1}\\
&\times\left(D^{-1}-\frac{\Delta_{\hat m}}{f^2}\right)+1\Bigg]\Bigg\}\frac{f^2}{2(\not p-\hat M)}.
\end{aligned} \tag{B11}$$

Using the proportionality relation between $X+Y_R$ and Y_L+Z given by Eq. (B9) we obtain the following expression for the on-shell $t(\not p)$ matrix:

$$t(\not{p})=X+Y_R+Y_L+Z=(Y_L+Z)\left[(\not{p}-\hat{M})^{-1}D^{-1}(\not{p}-\hat{M})\times\left(D^{-1}+\frac{\Delta_{\hat{m}}}{f^2}\right)^{-1}+1\right]. \quad \text{(B12)}$$

Inverting this equation and using Eq. (B11) we get finally the expression given in Eq. (28).

APPENDIX C: BEST FIT RESULTS

The best fit ($\chi^2/dof=0.75$) parameters are

$$J_{\pi N}=0.1897\pm0.0004,$$

$$J_{\eta N}=0.6206\pm0.0002,$$

$$J_{K\Lambda}=-1.227\pm0.003,$$

$$J_{K\Sigma}=-0.0143\pm0.005,$$

$$\Delta_{N,1}/(m_\pi+M_N)^2=0.776\pm0.002,$$

$$\Delta_{N,2}/(m_\eta+M_N)^2=1.8375\pm0.0004,$$

$$\Delta_\Lambda/(m_K+M_\Lambda)^2=-2.923\pm0.008, \quad \text{(C1)}$$

$$\Delta_\Sigma/(m_K+M_\Sigma)^2=1.000\pm0.017,$$

$$\Delta_\pi/(m_\pi+M_N)^2=-0.0123\pm0.0003,$$

$$\Delta_\eta/(m_\eta+M_N)^2=-0.1560\pm0.0002,$$

$$\Delta_{K,1}/(m_K+M_\Lambda)^2=-0.006324\pm0.000003,$$

$$\Delta_{K,2}/(m_K+M_\Sigma)^2=0.001128\pm0.000003.$$

The correlation matrix, defined as usual,

$$r_{ij}=\langle x_i x_j\rangle,$$

$$x_i=\frac{c_i-\langle c_i\rangle}{\sqrt{\langle c_i^2\rangle-\langle c_i\rangle^2}},$$

$$\langle f(c_1,\ldots,c_n)\rangle=\frac{1}{N}\sum_{\alpha=1}^{N} f(c_{1,\alpha},\ldots,c_{n,\alpha}), \quad \text{(C2)}$$

c_i being any of the 12 parameters $J's$ and $\Delta's$, turns out to be

$$\begin{pmatrix}
1.00 & & & & & & & & & & & \\
-0.62 & 1.00 & & & & & & & & & & \\
0.35 & 0.21 & 1.00 & & & & & & & & & \\
0.28 & -0.28 & 0.48 & 1.00 & & & & & & & & \\
0.67 & -0.22 & 0.57 & 0.09 & 1.00 & & & & & & & \\
0.63 & -0.35 & -0.18 & -0.15 & 0.00 & 1.00 & & & & & & \\
0.32 & 0.24 & 0.97 & 0.42 & 0.49 & -0.10 & 1.00 & & & & & \\
0.36 & -0.30 & 0.51 & 0.99 & 0.14 & -0.09 & 0.43 & 1.00 & & & & \\
0.50 & -0.51 & -0.30 & -0.08 & -0.21 & 0.91 & -0.25 & -0.04 & 1.00 & & & \\
-0.51 & 0.48 & -0.48 & -0.62 & -0.71 & 0.30 & -0.33 & -0.65 & 0.30 & 1.00 & & \\
0.10 & -0.37 & 0.12 & 0.20 & 0.56 & -0.59 & 0.01 & 0.18 & -0.55 & -0.77 & 1.00 & \\
0.19 & -0.03 & 0.54 & 0.48 & 0.67 & -0.56 & 0.42 & 0.48 & -0.69 & -0.84 & 0.72 & 1.00
\end{pmatrix}. \quad \text{(C3)}$$

The large correlations (0.97 and 0.99) between the pairs $J_{K\Lambda}-\Delta_\Lambda$ and $J_{K\Sigma}-\Delta_\Sigma$ can be understood by looking at Eq. (34) and taking into account the smallness of the parameters $\Delta_{K,1}$ and $\Delta_{K,2}$, respectively.

APPENDIX D: THE HEAVY BARYON LIMIT AND HBChPT

The study of the heavy baryon limit of the BSE amplitude given in Eq. (34) is, in principle, of theoretical and phenomenological interest. In the static limit, baryons behave like fixed sources, and consequently the two-particle problem should reduce to a one-particle scattering problem (in our case of meson-baryon scattering it would correspond to a Klein-Gordon equation with a spin-dependent potential). It has been known that the BSE has some difficulties in reproducing this heavy-light limit in certain situations (ladder approximation to one boson exchange [32]). We show below that our amplitude has a correct one particle limit due to the fact the *s*-wave interaction is of the contact type. If, in addition to a heavy baryon expansion, a chiral expansion in powers of $1/f^2$ is carried out, we should recover in this double expansion some form of the results found in Refs. [25,26,14] within HBChPT for the elastic πN scattering amplitude. The heavy baryon expansion may be taken by making the baryon

masses $\hat{M}\to\infty$ but keeping the meson masses, $\hat{m}$, and the meson momentum, q, finite. On the other hand, baryon mass splittings must be considered higher order effects, see, e.g., [19], so that we take the mass matrix

$$\hat{M}=M_B+\Delta\hat{M} \tag{D1}$$

with $M_B\to\infty$ the common mass of the baryon octet which is proportional to the identity matrix. Accordingly, in the πN elastic channel we take

$$\sqrt{s}=E+\omega=M_N+\omega+\frac{\omega^2-m_\pi^2}{2M_N}+\cdots, \tag{D2}$$

where $M_N=M_B+\Delta M_N$. In this appendix we match our amplitude to the HBChPT third order results of Ref. [14] based on the previous analysis of Refs. [25,26]. The heavy baryon expansion can be directly done for explicit variables, such as masses and c.m. energy $\sqrt{s}$. The constants $J_{\pi N},\ldots,\Delta_{N,1},\ldots,\Delta_\pi,\ldots$, given by our numerical fit in Eq. (C1), also might have a baryon mass dependence. Such a dependence should lead to some changes in the heavy baryon expansion which cannot be easily determined. In addition, given the nonperturbative nature of our solution and the fact that many aspects of the coupled channel meson-baryon data in the S_{11}–strangeness zero channel are described after unitarization up to energies as high as $\sqrt{s}=2$ GeV, it seems obvious that the parameters of Eq. (C1) also incorporate higher-order effects in the chiral expansion.

1. Static limit

It is convenient to do the study in terms of the inverse coupled channel matrix amplitude, $t^{-1}(s)$, given by Eq. (34). From the expression of the one-loop integral Eq. (A9) and Eq. (A10) we get to leading order

$$M\overline{J}_0(s,m,M)\big|_{\sqrt{s}=\sqrt{M_N^2+\omega^2-m_\pi^2}+\omega}=\frac{1}{16\pi^2}\log\left(\frac{M^2}{m^2}\right)(m-\omega)+\overline{K}_m(\omega)+\mathcal{O}\left(\frac{1}{M}\right). \tag{D3}$$

The subtraction point for the HBChPT integrals is $\omega=m$, $\overline{K}_m(m)=0$, and their explicit expression is

$$\overline{K}_m(\omega)=\frac{1}{8\pi^2}\begin{cases}-\sqrt{\omega^2-m^2}\,\operatorname{arccosh}\left(-\dfrac{\omega}{m}\right), & \omega<-m,\\ +\sqrt{m^2-\omega^2}\arccos\left(-\dfrac{\omega}{m}\right), & \omega^2<m^2,\\ +\sqrt{\omega^2-m^2}\left[\operatorname{arccosh}\left(\dfrac{\omega}{m}\right)-i\,\pi\right], & \omega>m.\end{cases} \tag{D4}$$

Thus, one obtains for the unsubtracted integral

$$\begin{aligned}MJ_0(s,m,M)\big|_{\sqrt{s}=\sqrt{M_N^2+\omega^2-m_\pi^2}+\omega}&=K_{mM}(\omega)+\mathcal{O}\left(\frac{1}{M}\right)\\&=MJ^0_{mM}+\frac{1}{16\pi^2}\log\frac{M^2}{m^2}(m-\omega)+\overline{K}_m(\omega)+\mathcal{O}\left(\frac{1}{M}\right),\end{aligned} \tag{D5}$$

where the HBChPT unsubtracted integrals $K_{mM}(\omega)$, fulfilling $K_{mM}(m)=MJ_{mM}$ and the heavy baryon approximation of the subtraction constant defined through Eq. (A8),

$$J_0[s=(m+M)^2]=J^0_{mM}\left\{1+\mathcal{O}\left(\frac{1}{M}\right)\right\} \tag{D6}$$

have been introduced. In the static limit we obtain from Eqs. (16) and (34) [$f(\omega)\to-t(s)/(4\pi)$]

$$f(\omega)^{-1}=8\pi\left[\overline{K}_{\hat{m}}(\omega)+\frac{1}{16\pi^2}\ln\frac{\hat{M}^2}{\hat{m}^2}(\hat{m}-\omega)+\hat{M}J^0_{\hat{m},\hat{M}}+\frac{\Delta^0_{\hat{m}\hat{M}}}{4\hat{M}}\right]-\frac{4\pi}{\omega}\left\{\Delta^0_{\hat{m}}-\left[\frac{2}{f^2}D+\frac{1}{f^4}D\Delta^0_{\hat{m}}D\right]^{-1}\right\} \tag{D7}$$

with $\overline{K}_{\hat{m}}(\omega)=\mathrm{Diag}[\overline{K}_\pi(\omega),\overline{K}_\eta(\omega),\overline{K}_K(\omega),\overline{K}_K(\omega)]$ and the heavy baryon approximation of the subtraction constants are defined by means of the expansion

$$\Delta_{\hat{m}}=\Delta^0_{\hat{m}}\left\{1+\mathcal{O}\left(\frac{1}{M}\right)\right\},$$

$$\Delta_{\hat{m}\hat{M}}=\Delta^0_{\hat{m}\hat{M}}\left\{1+\mathcal{O}\left(\frac{1}{M}\right)\right\}.$$

The Eq. (D7) corresponds, as it should, to a one-particle scattering problem, fulfilling the coupled channel unitarity condition

$$\mathrm{Im}\,f(\omega)^{-1}=-\sqrt{\omega^2-\hat{m}^2}\,\theta(\omega-\hat{m}). \tag{D8}$$

The pole in Eq. (D7) for the inverse amplitude is a static limit reminiscent from the baryonic Adler zero, $\sqrt{s}-\hat{M}=0$, of the lowest order potential. The constant combination appearing in the inverse amplitude, Eq. (D7), $\hat{M}J^0_{\hat{m}\hat{M}}+\Delta^0_{\hat{m}\hat{M}}/4\hat{M}$ should go to some definite value in the static limit, $M\to\infty$. In case it would diverge, the scattering amplitude would become trivial. We may try to estimate these constants using the numerical values obtained in the χ^2 fit carried out in this work and given in Eq. (C1). We get

$$M_NJ_{\pi N}+\frac{\Delta_{\pi N}}{4M_N}=-0.47m_\pi,$$

$$M_NJ_{\eta N}+\frac{\Delta_{\eta N}}{4M_N}=-1.08m_\eta,$$

$$M_\Lambda J_{K\Lambda}+\frac{\Delta_{K\Lambda}}{4M_\Lambda}=+0.67m_K,$$

$$M_\Sigma J_{K\Sigma}+\frac{\Delta_{K\Sigma}}{4M_\Sigma}=-1.24m_K \tag{D9}$$

in units of the relevant pseudoscalar meson masses. Though the numerical values used for the subtraction constants contain higher order effects in the heavy baryon expansion, we see that there is indeed some trend to cancellation, because the $J's$ and the $\Delta's$ contributions have opposite signs in the first three cases, and $J_{K\Sigma}$ is very small. Moreover, the constants do not seem to attain unnaturally large values, although it is hard to say which should be an accurate appropriate value.

2. Chiral and heavy baryon expansion

Expanding Eq. (34) in powers of $1/f^2$ we get

$$t(s)=t_2(s)+t_4(s)+\cdots, \tag{D10}$$

where

$$t_2(s)=\frac{1}{f^2}\{\sqrt{s}-\hat{M},D\}, \tag{D11}$$

$$t_4(s)=\frac{1}{f^4}(\sqrt{s}-\hat{M})D\frac{\Delta_{\hat{m}}}{\sqrt{s}-\hat{M}}D(\sqrt{s}-\hat{M})+\frac{1}{f^4}\{\sqrt{s}-\hat{M},D\}\times\left(\frac{(\sqrt{s}+\hat{M})^2-\hat{m}^2}{2\sqrt{s}}\hat{J}_0(s)-\frac{\Delta_{\hat{m}}}{\sqrt{s}-\hat{M}}+\frac{\Delta_{\hat{m}\hat{M}}}{2\sqrt{s}}\right)\times\{\sqrt{s}-\hat{M},D\}. \tag{D12}$$

In the heavy baryon limit we get for the elastic $\pi N\to\pi N$ amplitude in the S_{11} channel

$$f(\omega)=f_2(\omega)+f_4(\omega)+\cdots \tag{D13}$$

with

$$f_2(\omega)=+\frac{\omega}{4\pi f_\pi^2}-\frac{m_\pi^2+\omega^2}{8\pi f_\pi^2 M_N}+\frac{\omega(3m_\pi^2+\omega^2)}{16\pi f_\pi^2 M_N^2}+\mathcal{O}\left(\frac{1}{M_N^3 f^2}\right), \tag{D14}$$

$$f_4(\omega)=-\frac{\omega^2}{64\pi f_\pi^2}\left[\frac{16}{f_\pi^2}\left(2K_{\pi N}(\omega)+\frac{\Delta_{\pi N}}{2M_N}\right)+\frac{9}{f_K^2}\left(2K_{K\Lambda}(\omega)+\frac{\Delta_{K\Lambda}}{2M_\Lambda}\right)+\frac{1}{f_K^2}\left(2K_{K\Sigma}(\omega)+\frac{\Delta_{K\Sigma}}{2M_\Sigma}\right)\right]+\frac{3\omega}{256\pi f_\pi^2}\left[\frac{16}{f_\pi^2}\Delta_\pi+\frac{9}{f_K^2}\Delta_{K,1}+\frac{1}{f_K^2}\Delta_{K,2}\right]+\mathcal{O}\left(\frac{1}{M_N f^4}\right). \tag{D15}$$

In the region[18] $m_\pi\leqslant\omega\leqslant m_K$ only the $K_{\pi N}(\omega)$ has an imaginary part, to comply with perturbative elastic unitarity, whereas $K_{K\Lambda}(\omega)$ and $K_{K\Sigma}(\omega)$ are purely real. To write down this expression we have considered the prescription $D/f^2\to\hat{f}^{-1}D\hat{f}^{-1}$ given in Eq. (9). At threshold, $\omega=m_\pi$, the πN scattering length in this channel reads

$$a_{\pi N}=\frac{m_\pi}{4\pi f_\pi^2}-\frac{m_\pi^2}{4\pi f_\pi^2 M_N}+\frac{m_\pi^3}{4\pi f_\pi^2 M_N^2}-\frac{m_\pi^2}{64\pi f_\pi^2}\left(\frac{16}{f_\pi^2}\left[2M_N J^0_{\pi N}+\frac{\Delta^0_{\pi N}}{2M_N}\right]+\frac{9}{f_K^2}\left[2M_\Lambda J^0_{K\Lambda}+\frac{\Delta^0_{K\Lambda}}{2M_\Lambda}+\frac{1}{4\pi^2}\left\{(m_\pi-m_K)\log\frac{M_\Lambda}{m_K}+\sqrt{m_K^2-m_\pi^2}\arccos\left(-\frac{m_\pi}{m_K}\right)\right\}\right]+\frac{1}{f_K^2}\left[2M_\Sigma J^0_{K\Sigma}+\frac{\Delta^0_{K\Sigma}}{2M_\Sigma}+\frac{1}{4\pi^2}\left\{(m_\pi-m_K)\log\frac{M_\Sigma}{m_K}+\sqrt{m_K^2-m_\pi^2}\arccos\left(-\frac{m_\pi}{m_K}\right)\right\}\right]\right)+\frac{3m_\pi}{256\pi f_\pi^2}\left[\frac{16}{f_\pi^2}\Delta^0_\pi+\frac{9}{f_K^2}\Delta^0_{K,1}+\frac{1}{f_K^2}\Delta^0_{K,2}\right]+\mathcal{O}\left(\frac{1}{f^2M_N^3},\frac{1}{M_N f^4},\frac{1}{f^6}\right). \tag{D16}$$

From Eq. (D15) and Eq. (D16) above it is clear that there is no contribution from the ηN channel to this $1/f^4$ order of approximation. This is a direct consequence of the structure of the coupled channel matrix D given by Eq. (8) since the corresponding $\pi N\to\eta N$ transition matrix element vanishes in the Born approximation. For this reason, the channel ηN starts contributing at order $1/f^6$. This situation is unexpected, because on general grounds we expect the ηN channel to be more important at low energies than the $K\Lambda$ and $K\Sigma$ channels since their thresholds lie at higher energies. Using the numerical values of the coefficients obtained from the fit of

[18]Note, that the ηN channel appears at order $1/f^6$.

Eq. (C1) to estimate the scattering length, Eq. (D16), we get

$$a_{\pi N}=\underbrace{0.22}_{1/f^2}+\underbrace{\overbrace{0.22}^{\pi N}-\overbrace{1.06}^{K\Lambda}+\overbrace{0.18}^{K\Sigma}}_{1/f^4}=-0.43\ \text{fm} \tag{D17}$$

which should be compared to the one of Eq. (38) obtained from the full amplitude, 0.179 fm. Obviously, the different values should be attributed to non-negligible higher order effects, which in particular include ηN contributions, and higher order corrections to the J^0 and Δ^0 coefficients. This is very reassuring because the full BSE amplitude, Eq. (34), besides restoring unitarity automatically includes all orders in the chiral expansion.

3. Matching to HBChPT

The S_{11} partial wave amplitude deduced from the work of Ref. [14] based in HBChPT to third order [25,26] reads, after straightforward angular integration,

$$f_2(\omega)=\frac{\omega}{4f_\pi^2\pi}+\frac{m_\pi^4 g_A^2+\omega^2 m_\pi^2[-6-48a_3+4g_A^2]+\omega^4[-6+48(a_1+a_2)-5g_A^2]}{48f_\pi^2 M_N\pi\omega^2}$$
$$+\frac{m_\pi^6 g_A^2-g_A^2\omega^2 m_\pi^4+\omega^4 m_\pi^2[6-48(a_2-2a_3)-7g_A^2]+\omega^6[6-48a_1+7g_A^2]}{48f_\pi^2 M_N^2\pi\omega^3}, \tag{D18}$$

$$f_4(\omega)=-\frac{\omega^2\overline{K}_\pi(\omega)}{2\pi f_\pi^4}+\frac{1}{5760f_\pi^4\pi^3}\{-102m_\pi^3 g_A^2\pi+\omega m_\pi^2[-130+1440\tilde{b}_6-230g_A^2]+144g_A^2\pi m_\pi\omega^2$$
$$+\omega^3[115+720(\tilde{b}_1+\tilde{b}_2+\tilde{b}_3)-205g_A^2]\}+\frac{13g_A^2 m_\pi^5}{3840f_\pi^4\pi^2(m_\pi^2-\omega^2)}\log\left(\frac{\omega^2}{m_\pi^2}\right)+\frac{(1+g_A^2)m_\pi^4\omega}{128f_\pi^4\pi^3(\omega^2-m_\pi^2)}\left[\operatorname{arccosh}\left(\frac{\omega}{m_\pi}\right)\right]^2$$
$$+\frac{\omega^2[3(1+g_A^2)m_\pi^2+2\omega^2(1+5g_A^2)]}{192f_\pi^4\pi^3\sqrt{\omega^2-m_\pi^2}}\operatorname{arccosh}\left(\frac{\omega}{m_\pi}\right)+\frac{g_A^2(13m_\pi^4-46\omega^2m_\pi^2+48\omega^4)}{1920f_\pi^4\pi^2\sqrt{\omega^2-m_\pi^2}}\arctan\left(\frac{\sqrt{\omega^2-m_\pi^2}}{m_\pi}\right). \tag{D19}$$

There is no unique way to match the low energy chiral expansion of the coupled channel BSE amplitude, Eq. (D15), to the third order HBChPT calculation of Refs. [25,26], Eq. (D19). The analytical structure is different besides the elastic unitarity cut at $\omega=m_\pi$ which turns out to coincide. Indeed, while the former presents the inelastic unitarity cuts for the considered $K\Lambda$ and $K\Sigma$ coupled channels, the latter includes perturbatively the left-hand cut at $\omega=0$. Obviously, any particular choice of the matching point generates a specific set of low energy constants. After explicitly separating the elastic unitarity correction of both amplitudes, it seems reasonable to do the matching of the remaining pieces in a polynomial expansion around the elastic threshold point, $\omega=m_\pi$, since neither inelastic unitarity cuts nor the left cut are expected to be crucial at that point. Instead, we expect both amplitudes to provide a sensible approximation. Also, direct inspection of Eq. (D15) and Eq. (D19) reveals that only some additive combinations among renormalization constants can be established. In particular, in Eq. (D15) there are two independent combinations of low energy constants. Thus, it proves sufficient to Taylor expand around $\omega=m_\pi$ up to first order. Using the numerical values for the input parameters, Eq. (37), in Eq. (D15) and the numerical values for the parameters in Ref. [14] in Eq. (D19) the following identifications hold (in units of fm):

$$0.185=0.175+22.8\overline{\Delta}^0_\pi+2.51\overline{\Delta}^0_{N,1}+17.3\overline{\Delta}^0_{K,1}+1.57\overline{\Delta}^0_\Lambda$$
$$+2.12\overline{\Delta}^0_{K,2}+0.179\overline{\Delta}^0_\Sigma-7.60J^0_{\pi N}-3.01J^0_{K\Lambda}$$
$$-0.357J^0_{K\Sigma},$$

$$-0.051=0.163+20.3\overline{\Delta}^0_\pi+5.01\overline{\Delta}^0_{N,1}+15.7\overline{\Delta}^0_{K,1}+3.14\overline{\Delta}^0_\Lambda$$
$$+1.94\overline{\Delta}^0_{K,2}+0.359\overline{\Delta}^0_\Sigma-15.2J^0_{\pi N}-6.01J^0_{K\Lambda}$$
$$-0.714J^0_{K\Sigma}, \tag{D20}$$

where $\overline{\Delta}^0_{\hat{m}}=\Delta^0_{\hat{m}}/(m+M)^2$ and $\overline{\Delta}^0_{\hat{M}}=\Delta^0_{\hat{M}}/(m+M)^2$ are dimensionless. As we see, there is a large degree of redundancy when the matching is performed considering only these low orders of the expansion. By using the values of Eq. (C1), to estimate the heavy-baryon mass independent parameters appearing in the right-hand side of the two relations established in Eq. (D20), we obtain -0.43 and -0.618, re-

spectively. The disagreement, with respect to the left-hand side values, is not completely surprising because the numerical values used for the subtraction constants contain higher order effects in the heavy baryon expansion. Besides, the nominally small differences $[\mathcal{O}(1/M)]$ between $\bar{\Delta}^0$'s and J^0's and $\bar{\Delta}$'s and J's might lead to significant numerical changes because the factors multiplying these constants are large in units of the left-hand-side values of Eq. (D20).

[1] L. Ya. Glozman and D. O. Riska, Phys. Lett. B **366**, 305 (1996); Phys. Rep. **268**, 263 (1996).
[2] T. P. Vrana, S. A. Dytman, and T. S. H. Lee, Phys. Rep. **328**, 181 (2000).
[3] N. Kaiser, P. B. Siegel, and W. Weise, Nucl. Phys. **A594**, 325 (1995); Phys. Lett. B **362**, 23 (1995).
[4] J. Caro Ramon, N. Kaiser, S. Wetzel, and W. Weise, Nucl. Phys. **A672**, 249 (2000).
[5] V. Bernard, N. Kaiser, and U.-G. Meißner, Nucl. Phys. **A619**, 261 (1997); N. Fettes, V. Bernard, and U.-G. Meißner, *ibid.* **A669**, 269 (2000).
[6] E. Oset and M. J. Vicente Vacas, Nucl. Phys. **A446**, 584 (1985).
[7] T. S. Jensen and A. F. Miranda, Phys. Rev. C **55**, 1039 (1997).
[8] M. Batinić, I. Šlaus, A. Švarc, and B. M. K. Nefkens, Phys. Rev. C **51**, 2310 (1995); **57**, 1004 (1998).
[9] J. C. Nacher, A. Parreño, E. Oset, A. Ramos, A. Hosaka, and M. Oka, Nucl. Phys. **A678**, 187 (2000).
[10] E. Oset (private communication).
[11] J. Nieves and E. Ruiz Arriola, Phys. Lett. B **455**, 30 (1999); Nucl. Phys. **A679**, 57 (2000).
[12] J. Nieves and E. Ruiz Arriola, Phys. Rev. D **63**, 076001 (2001).
[13] A. Gómez Nicola and J. R. Peláez, Phys. Rev. D **62**, 017502 (2000).
[14] J. Nieves and E. Ruiz Arriola, hep-ph/0001013; A. Gómez Nicola, J. Nieves, J. R. Peláez, and E. Ruiz Arriola, Phys. Lett. B **486**, 77 (2000).
[15] M. Knecht, B. Moussallam, J. Stern, and N. H. Fuchs, Nucl. Phys. **B457**, 513 (1995); **B471**, 445 (1996).
[16] J. Bijnens, G. Colangelo, G. Ecker, J. Gasser, and M. E. Sainio, Phys. Lett. B **374**, 210 (1996); Nucl. Phys. **B508**, 263 (1997).
[17] N. Fettes and Ulf. G. Meißner, Nucl. Phys. **A676**, 311 (2000).
[18] E. Ruiz Arriola, A. Gómez Nicola, J. Nieves, and J. R. Peláez, Proceedings of the ''Miniworkshop on Few Quark Problems,'' Bled, Slovenia, 2000, hep-ph/0011164.
[19] A. Pich, Rep. Prog. Phys. **58**, 563 (1995).
[20] W. M. Gibson and B. R. Pollard, *Symmetry Principles in Elementary Particle Physics* (Cambridge University Press, Cambridge, England, 1976).
[21] T. Ericson and W. Weise, *Pions and Nuclei* (Clarendon Press, Oxford, 1988).
[22] R. A. Arndt, I. I. Strakovsky, R. L. Workman, and M. M. Pavan, Phys. Rev. C **52**, 2120 (1995).
[23] A. Baldini *et al.*, in *Numerical Data and Functional Relationships in Science and Technology. Grp. 1: Nuclear and Particle Physics*, Landolt-Börnstein Vol. 12a (Springer, Berlin, 1988).
[24] H.-Ch. Schröder *et al.*, Phys. Lett. B **469**, 25 (1999).
[25] M. Mojzis, Eur. Phys. J. C **2**, 181 (1998).
[26] N. Fettes, U.-G. Meißner, and S. Steininger, Nucl. Phys. **A640**, 199 (1998).
[27] Particle Data Group, C. Caso *et al.*, Eur. Phys. J. C **3**, 1 (1998).
[28] S. Mandelstam, Phys. Rev. **112**, 1344 (1958).
[29] J. Nieves and E. Ruiz Arriola (unpublished).
[30] T. Becher and H. Leutwyler, J. High Energy Phys. **06**, 017 (2001); Eur. Phys. J. C **9**, 643 (1999).
[31] A. Ramos, talk at NSTAR2001, Workshop on The Physics of Excited Nucleons, Mainz, Germany, 2001.
[32] F. Gross, Phys. Rev. C **26**, 2203 (1982).